Article:
Wei, Y, Wang, C, Liu, X et al. (6 more authors) (2020) Impact of microfluidization and thermal treatment on the structure, stability and in vitro digestion of curcumin loaded zein-propylene glycol alginate complex nanoparticles. Food Research International, 138 (Part B). 109817. ISSN 0963-9969

https://doi.org/10.1016/j.foodres.2020.109817

Impact of microfluidization and thermal treatment on the structure, stability and in vitro digestion of curcumin loaded zein-propylene glycol alginate complex nanoparticles

*Yang Wei[a, b], Chao Wang[a], Xin Liu[a], Alan Mackie[b], Liang Zhang[a], Jinfang Liu[a], Like Mao[a], Fang Yuan[a], Yanxiang Gao[a]**

[a]*Beijing Advanced Innovation Center for Food Nutrition and Human Health, Beijing Laboratory for Food Quality and Safety, Beijing Key Laboratory of Functional Food from Plant Resources, College of Food Science & Nutritional Engineering, China Agricultural University, Beijing, 100083, P. R. China*

[b]*Food Colloids and Processing Group, School of Food Science and Nutrition, University of Leeds, Leeds LS2 9JT, UK*

*Corresponding author.

Tel.: + 86-10-62737034

Fax: + 86-10-62737986

Address: Box 112, No.17 Qinghua East Road, Haidian District, Beijing 100083, China

E-mail: gyxcau@126.com

Abstract:

The aim of this study was to modulate the physicochemical properties, molecular interactions and microstructure of zein-propylene glycol alginate (PGA) complex nanoparticles for delivery of curcumin with the aid of high pressure microfluidization (HPM) (50-150 MPa) and thermal treatment (45-85 ℃). The size of zein-PGA complex nanoparticles was decreased to around 300 nm. It was confirmed that the pressure of 100 MPa and temperature of 75 ℃ were the optimum parameters to provide a better protection of entrapped curcumin against environmental stresses. The electrostatic interaction, hydrogen bonding and hydrophobic attraction were the dominant driving forces in the formation of the complex nanoparticles. Field emission scanning electron microscopy (FE-SEM) revealed that HPM and thermal treatment facilitated the complex nanoparticles to form a more uniform size and spherical shape. During *in vitro* gastrointestinal digestion, zein-PGA complex nanoparticles showed excellent gastric stability and sustained-release of curcumin in the small intestine. HPM and thermal treatment showed a synergistic effect on enhancing the bioaccessibility of curcumin entrapped in zein-PGA complex nanoparticles. The findings revealed the influence of HPM and thermal treatment on functional attributes of the complex nanoparticles, which could be utilized to design food grade nanoparticles with desirable stability and digestive properties.

Key words: Zein-PGA complex nanoparticles; Curcumin; High-pressure microfluidization; Thermal treatment; Physicochemical stability; *In vitro* digestion

1. Introduction

Food nanoparticles have gained considerable attention due to their benefical characteristics including biocompatibility, biodegradability, and mucoadhesive ability, which can be utilized to deliver bioactives through improving water solubility, chemical stability and bioavailability (Semenova, 2017). Proteins are the most important biomaterials to produce food nanoparticles, which are regarded as environmentally sustainable with high nutritional values. Nevertheless, the protein-based colloids usually lose their structural stability when the physiological pH is close to isoelectric point (pI) or under extreme stresses (heat, high pressure or salts). Most of proteins can be digested by proteases in the stomach and the bioactives entrapped would be released (McClements & Gumus, 2016). To improve the stability of nanocarriers, polysaccharides are usually introduced to coat the protein particles as a shell or interact with proteins to fabricate stable hybrid nanoparticles (Huang et al., 2017; Joye, Davidov-Pardo, & McClements, 2015). The presence of polysaccharides provides the steric and electrostatic repulsion among the colloidal particles, preventing aggregation and sedimentation and modulating the release and adsorption of nutraceuticals loaded during gastrointestinal digestion.

The modification of proteins to broaden their application has been widely reported, such as induction of heat, high pressure, enzymes and ionic gelation. High pressure processing and thermal treatment are the most important strategies to modulate the properties of biopolymers, which are widely utilized in industrial applications. High

pressure microfluidization (HPM) has been utilized to modulate the functional attributes of various water-soluble proteins, including whey protein (Dissanayake & Vasiljevic, 2009), peanut protein (Hu, Zhao, Sun, Zhao, & Ren, 2011), and soy protein (Song, Zhou, Fu, Chen, & Wu, 2013). Besides, researchers reported that thermal processing was utilized to modify structural properties of alcohol-soluble proteins (zein). Zein is a plant protein extracted from corn, which is a promising biomaterial for several industrial applications (Paliwal & Palakurthi, 2014). As reported by previous researchers, zein can be well dissolved in 50%-90% (v/v) aqueous ethanol solutions (Shukla & Cheryan, 2001). It can be self-assembled into films, fibers, microspheres and nanoparticles due to its highly hydrophobic amino acid proportion (Momany et al., 2006; Shukla & Cheryan, 2001; Wei, Sun, Dai, Zhan, & Gao, 2018; Wei, Yu, et al., 2020). Propylene glycol alginate (PGA) is a kind of polysaccharide with surface-activity attributed to its propylene glycol groups, which can interact with zein to form the stable complexes for delivery of bioactives (Wei, Yu, et al., 2019).

Most of the previous efforts on adjusting the molecular structure of zein to improve its functional properties focused on adjusting the degree of protein aggregation, structure, and rheological properties through adjusting the ethanol concentration and pH of the solvent where the prolamin was dissolved (Kim & Xu, 2008; Selling, Hamaker, & Sessa, 2007; Zhang, Luo, & Wang, 2011). Additionally, they investigated the influence of temperature on the conformation of zein and found that the alteration of zein structure mainly occurred at 70 ℃ (Selling et al., 2007). Microfluidization could also be incorporated into the protein modification, which influenced the hydrogen

bonding and hydrophobic interactions among the protein-protein or protein-polysaccharide complexes through high pressure, shear stress, turbulence and cavitation (Ye & Harte, 2014). Based on a previous work, the combined thermal treatment with HPM was confirmed to alter the physicochemical and conformational properties of zein (Sun, Dai, Liu, & Gao, 2016). Nevertheless, there is no information available about the influence of the coupled treatments of heating and HPM on the functional attributes, environmental stability and *in vitro* digestion of protein-polysaccharide binary complex nanoparticles for delivery of nutraceuticals. The objective of this study was to investigate the potential of heating and HPM applied in the development of nanoparticle-based delivery vehicles.

In this study, curcumin was chosen as a model polyphenolic compound to be encapsulated into the zein-PGA complex nanoparticles through the emulsification-evaporation method. Different microfluidization pressures (50-150 MPa) and heating temperatures (45-85 ℃) were utilized to modulate the physicochemical, conformational and morphological properties of the complex nanoparticles. The stability of complex nanoparticles was assessed systematically under various environmental stresses (light, heat, pH and salts). The conformational alteration, secondary structure of zein, intermolecular interactions and thermal behavior were analyzed to reveal the formation mechanism of the complex nanoparticles. The release percentage and bioaccessibility of curcumin loaded in complex nanoparticles were appraised during the simulated gastrointestinal (GI) tract.

2. Materials and methods

2.1. Materials

Zein (CAS: 9010-66-6) with a protein content of 91.3%, pepsin (pack size: P7012), pancreatin (pack size: P1750) and bile salts (pack size: 48305) were purchased from Sigma-Aldrich (St. Louis, MO, USA). It has been reported that pepsin activity was greater than 2500 units/mg protein. The bile salts were composed of 50% deoxycholic acid sodium salt and 50% cholic acid sodium salt. Propylene glycol alginate (PGA) (CAS: 9005-37-2) (esterification: 87.9%) was kindly provided by Hanjun Sugar Industry Co. Ltd. (Shanghai, China). Curcumin (>98%) (CAS: 458-37-7) was obtained from Adamas-Beta (Shanghai, China). Absolute ethanol (99.99%), solid sodium hydroxide and liquid hydrochloric acid (36%, w/w) were acquired from Eshowbokoo Biological Technology Co., Ltd. (Beijing, China).

2.2. Preparation of curcumin loaded zein-PGA complex nanoparticles

Briefly, 0.60 g of zein, 0.30 g of PGA and 0.10 g of curcumin were added into 160 mL 70% (v/v) aqueous ethanol solution in sequence to form the mixed solution with magnetic stirring under 600 rpm at 25 ℃ until their complete dissolution.

To investigate the influence of HPM pressure on the attributes of curcumin loaded zein-PGA binary complexes, the mixed solutions were subjected to microfluidization at 50, 75, 100, 125 and 150 MPa for 2 cycles at 25 ℃ by a Microfluidizer® processor model M-110EH (Microfluidics, Newton, MA, USA) (Sun, Dai, Liu, et al., 2016). All the solutions were then evaporated at 45 ℃ for 40 min to remove the ethanol and the

remaining volume was set to around 40 mL, which was then diluted with distilled water (pH 4.0) to 100 mL. The particle suspensions were centrifuged (Sigma 3k15, DJB labcare, Buckinghamshire, UK) at 725 × g for 10 min to remove large particle aggregates and unentrapped curcumin. The supernatants were collected. Thereafter, part of samples was placed at 5 ℃ for further analysis and the other part was freeze-dried for 48 h to obtain powder samples. The samples were termed as ZP-50MPa, ZP-75MPa, ZP-100MPa, ZP-125MPa and ZP-150MPa, respectively.

To investigate the influence of thermal treatment and HPM pressure on the properties of curcumin loaded zein-PGA binary complexes, the mixed solutions (0.60 g of zein, 0.30 g of PGA and 0.10 g of curcumin in 160 mL 70% (v/v) aqueous ethanol) were placed in a thermostatic water bath for 30 min at 45, 55, 65, 75 and 85 ℃. Thereafter, the solutions were subjected to microfluidization at 100 MPa for 2 cycles immediately. The following procedure of the nanoparticle dispersions was performed as the aforementioned process. The samples were termed as ZP-45℃, 100MPa, ZP-55℃, 100MPa, ZP-65℃, 100MPa, ZP-75℃, 100MPa and ZP-85℃, 100MPa.

As the controls, zein nanoparticles, zein nanoparticles with the combined microfluidization and thermal treatment, curcumin loaded zein nanoparticles, curcumin loaded zein nanoparticles with the combined microfluidization and thermal treatment and curcumin loaded zein-PGA complex nanoparticles without any processing were prepared by following the same procedure as aforementioned, which were termed as Z, Z-75℃,100MPa, Z-cur, Z-cur-75℃,100MPa and ZP, respectively. Besides, the samples with individual heating (75 ℃, 0MPa) and HPM (25 ℃, 100 MPa) processing were

prepared and named as ZP-75℃ and ZP-100MPa.

2.3. Particle size distribution and zeta-potential

Particle size and zeta-potential of the particle dispersions were determined by using a Nano-ZS90 (Zetasizer, Malvern Instruments Ltd., Worcestershire, UK). Stokes-Einstein equation and Smoluchowski model were used in the calculation of particle size and zeta potential, respectively. The samples were diluted 10 times with pH-adjusted distilled water (pH 4.0) to avoid multiple light-scattering effect. The type of cuvette used was DTS1060 and the scattering angle was 90°. The refractive index (RI) of water was set as 1.45 and the RI of the complex nanoparticles was set as 1.52. All the measurements were carried out at 25 ℃ in triplicate.

2.4. Encapsulation efficiency and loading capacity

The content of curcumin entrapped in the complex nanoparticles was determined by following our previous method (Dai, Wei, et al., 2018a). Briefly, 1 mL of freshly prepared particle dispersions was mixed with 4 mL ethanol through vortex oscillation for 2 min. Each sample was centrifuged at a speed of 10,000 × g for 30 min and the supernatant was collected. Thereafter, the curcumin in the supernatant was diluted to an appropriate concentration (0-6 μg/mL) with 80% aqueous ethanol solution (v/v). Absorbance was measured with a UV-1800 spectrophotometer (Shimadzu Corporation, Kyoto, Japan) at 426 nm. The concentration of curcumin was obtained by referring to a standard curve (R^2=0.999) of curcumin prepared under the same condition.

Encapsulation efficiency (EE) and loading capacity (LC) were calculated by

following equations 1 and 2 below:

$$\mathrm{EE}\ (\%) = \frac{\text{entrapped curcumin (mg)}}{\text{total curcumin input (mg)}} \times 100 \quad (1)$$

$$\mathrm{LC}\ (\%) = \frac{\text{entrapped curcumin (mg)}}{\text{total weight of zein,PGA,TS and curcumin input (mg)}} \times 100 \quad (2)$$

Entrapped curcumin means the total content of curcumin encapsulated into the complex nanoparticles. Total curcumin input means the total content of curcumin used during preparation of the nanoparticles.

2.5. Physicochemical stability

2.5.1. Physical stability

The physical stability of all the particle dispersions was estimated with the LUMiSizer (LUM GmbH, Berlin, Germany) based on the principle that the centrifugation accelerates the instability phenomenon (Sobisch & Lerche, 2008). The parameters used in the measurement were adapted as follows: 1.8 mL of colloidal dispersion; rotational speed, 3000 rpm; performed time, 3600 s; time interval, 20 s; temperature, 25 ℃.

2.5.2. Photostability

The photostability of curcumin in the complex particles against UV photolysis was tested. Briefly, 20 mL of freshly prepared complex particles was placed into transparent glass vial. Then samples were put into a controlled light cabinet (Q-Sun, Q-Lab Corporation, Ohio, USA) for up to 2 h under the exposing light condition (40 ℃, 0.35 W/m^2) (Wei, Yu, et al., 2019). The remaining curcumin was determined as described in section 2.4. The retention rate of curcumin was plotted against time.

2.5.3. Thermal stability

Briefly, 5 mL of freshly prepared curcumin loaded complex particles was placed into transparent glass vial and incubated in water bath at 85 ℃ for 30 min and then cooled down to 25 ℃ (Wei et al., 2018). The retention rate of curcumin was measured as described in section 2.4.

2.5.4. pH stability

Freshly prepared particle dispersions were adjusted to pH 2, 6 and 9 using 1 M NaOH or HCl (Wei, Yu, et al., 2019). After stored for 24 h at 25 ℃, the particle size and zeta-potential were measured as described in section 2.3.

2.5.5. Ionic stability

Freshly prepared particle dispersions were mixed with different quantities of NaCl powder for 2 h to ensure full interaction between the complex nanoparticles and different ions. The NaCl concentration in different samples was adjusted to 10, 50, and 100 mM, respectively (Dai, Wei, et al., 2018a). After storage for 24 h, the particle size and zeta-potential were measured as described in section 2.3.

2.6. Storage stability

Freshly prepared particle dispersions were incubated in temperature-controlled chambers (4, 37 and 55 ℃) for one week (Wei, Yang, et al., 2020). The particle size and retention rate of curcumin in the complex nanoparticles were measured after 7 days as described in section 2.3 and 2.4.

2.7. Fluorescence spectroscopy

Fluorescence of the particle dispersions was determined through a fluorescence spectrophotometer (F-7000, Hitachi, Tokyo, Japan). The excitation wavelength was set at 280 nm, and the emission spectra were collected between 290 and 450 nm with a scanning speed of 100 nm/min (Sun, Wei, Li, Dai, & Gao, 2017a). Intrinsic fluorescence of the protein was measured at a constant concentration of 0.2 mg/mL. All data were collected at 25 ℃, and each emission spectrum was the average of three runs.

2.8. Circular dichroism (CD) spectroscopy

The far-UV CD spectra (190-250 nm) were recorded using a CD spectropolarimeter (Pistar π-180, Applied Photophysics Ltd., Surrey, UK) (Wei et al., 2018). After a proper dilution of samples, the protein concentration was 0.2 mg/mL and path length was 0.1 cm with constant nitrogen flush during data acquisition. Ellipticity was recorded at a rate of 100 nm/min, 0.2 nm resolution, 20 accumulations, and 2.0 nm bandwidth.

2.9. Fourier transform infrared spectroscopy (FTIR)

FTIR was applied to characterize the vibration of functional groups of zein, PGA, curcumin and curcumin loaded binary complexes. Infrared spectra of freeze-dried powders were recorded using a Spectrum 100 Fourier transform spectrophotometer (PerkinElmer, Waltham, MA, USA). The spectra were acquired after 64 scans at a wavenumber range from 4000 to 400 cm^{-1} with a 4 cm^{-1} resolution (Wei et al., 2018).

2.10. X-ray diffraction (XRD)

The molecular arrangement of samples was measured by an X-ray diffractometer (Brucker D8, Odelzhausen, Germany) with a Cu anode, 40 kV voltage and current of 40 mA. The 2θ scan was fixed at 3 ° to 40 ° with a step size of 0.02 °and step time of 5 s (Huang et al., 2017).

2.11. Field emission scanning electron microscopy (FE-SEM)

The morphology of samples was observed using a field emission scanning electron microscopy (FE-SEM, SU8010, Hitachi, Tokyo, Japan). The samples were put on a double-sided adhesive coated with a thin layer of gold and measured under 20.0 kV acceleration voltage (Wei, Yu, et al., 2019).

2.12. In vitro gastrointestinal digestion and bioaccessibility of curcumin

All samples were digested with simulated gastric fluids (SGF) and simulated intestinal fluids (SIF) according to the international digestion protocol (Minekus et al., 2014). The pH value of SGF was adjusted to 2.0 using 1 M HCl and 30 mL of the particle dispersion was incubated at 37 ℃ for 1 h with 60 mL of SGF. The pH value of gastric digesta and SIF was adjusted to pH 7.0 using 1 M NaOH. After the digestion in stomach phase, 40 mL of gastric digesta was mixed with 40 mL of SIF and incubated for 2 h at 37 ℃.

Determinations of particle size, curcumin release percentage and microstructure

were carried out after samples were exposed to each stage. The curcumin release percentage was determined after each phase of digestion (Fan, Liu, Gao, Zhang, & Yi, 2018). An aliquot of raw digesta was centrifuged at 10000 rpm for 30 min at 10 ℃, and the supernatant was filtered with a 0.45 μm filter. Thereafter, the amount of curcumin released from each sample was determined as described in section 2.4. The curcumin release percentage (%) was calculated by following equation 3:

$$\text{Release percentage}\ (\%) = \frac{\text{released curcumin (mg)}}{\text{entrapped curcumin (mg)}} \times 100 \qquad (3)$$

The bioaccessibility of curcumin was determined after the intestinal digestion. Part of the digesta was processed using a high-speed centrifuge at 15,000 rpm for 60 min at 4 ℃ and the micelle phase containing the solubilized curcumin was collected. The bioaccessibility of curcumin was defined as the fraction of curcumin released from the food matrix and solubilized within mixed micelles present in the small intestine before it could be absorbed (Yao, Xiao, & McClements, 2014). The curcumin contents extracted from the initial nanoparticles and micelle fraction were determined according to the method described in section 2.4. The bioaccessibility (%) of curcumin was calculated by following equation 4:

$$Bioaccessibility\ (\%) = \frac{C_{micelle}}{C_{initial\ nanoparticle}} \times 100 \qquad (4)$$

where $C_{micelle}$ represented the concentration of curcumin in the micelle fraction and $C_{initial\ nanoparticle}$ represented the total concentration of curcumin encapsulated into the complex nanoparticles.

2.13. Statistical analysis

All the data obtained were average values of triplicate determinations and subjected to statistical analysis of variance using SPSS 18.0 for Windows (SPSS Inc., Chicago, USA). Statistical differences were determined by one-way analysis of variance (ANOVA) with Duncan's post hoc test and least significant difference ($p<0.05$) was accepted among the treatments.

3. Results and discussion

3.1. Particle size and zeta-potential

The effects of HPM, heating and the combined treatments on the size and charge properties of zein-PGA complex nanoparticles were evaluated. As shown in Fig. 1A, the largest size (580.7 ± 12.2 nm) was observed in ZP without any external processing. With the aid of HPM, the particle size was significantly ($p<0.05$) reduced in ZP-50MPa (320.6 ± 5.1 nm). With the rise in pressure level, the particle size was slightly decreased and the smallest size was obtained in ZP-125MPa (299.3 ± 7.8 nm), which demonstrated that HPM induced a reduction in the size of the complex nanoparticles. As reported previously, the appropriate pressure might dissociate the aggregates of zein molecules into smaller fragments, but higher pressure could result in the aggregation of zein molecules (Sun, Yang, et al., 2016). A similar phenomenon was found in several water soluble proteins, such as β-lactoglobulin (Zhong et al., 2014), soy protein (Song et al., 2013) and peanut protein (Hu et al., 2011). In our study, HPM showed a more significant effect on the formation process of the complex nanoparticles through the emulsification-evaporation method. At the higher pressure, the protein molecules were

partially unfolded and exposed more active sites, which fully interacted with and bound to the polysaccharide to form the compact and stable complexes. Therefore, compared to zein nanoparticles, there was a more noticeable reduction in the size of zein-PGA complex nanoparticles. However, irregular fluctuation occurred in the zeta-potential of the complex nanoparticles as the pressure was elevated.

At the fixed homogenization pressure, the impact of different heating temperatures on the size of zein-PGA complex nanoparticles was investigated (Fig. 1B). An obvious increase in the particle size was observed after thermal processing. All the samples exhibited a noticeable elevation in the particle size after heating at different temperatures. After heating at 45 ℃ for 30 min, the size of zein-PGA complex nanoparticles was increased from 318.4 ± 6.0 nm to 372.4 ± 14.9 nm. When the heating temperature was elevated continuously, the size of zein-PGA complex nanoparticles was increased slightly. Based on the previous studies, heating was generally used in combinaton with other treatments to promote the alteration in protein structure and improvement of functional properties, but the effect of thermal treatment alone was very limited (Kim & Xu, 2008; Selling et al., 2007; Zhang et al., 2011). In the relevant article, Sun et al. (2016) explored the influence of different heating temperatures on the formation of zein colloidal particles. The result showed that the increase in temperature from 75 to 95 °C had no significant effect on the size and microstructure of zein nanoparticles. This phenomenon was consistent with the findings of this study: Although thermal treatment could promote the aggregation and structural transformation of the complex nanoparticles, the increasing temperature showed a

limited impact on the complex nanoparticles. Besides, according to our previous research, the incorporation of PGA could effectively enhance the thermal stability of zein and form more stable complex nanoparticles, thereby reducing the effect of elevated temperature (Sun, Wei, Li, Dai, & Gao, 2017c; Wei et al., 2018).

Fig. 1C showed the influence of simultaneous HPM and thermal treatment on the particle size and zeta-potential of the control group. After the combined treatment, the size of most of nanoparticles was decreased significantly (p<0.05) except single zein nanoparticles without curcumin. As aforementioned, HPM induced a reduction in the particle size, but thermal treatment conversely promoted the particle aggregation. The phenomenon demonstrated that HPM had a dominant impact on the size of zein-PGA complex nanoparticles with the combination of HPM and heating. The external processing exhibited a more significant impact on the size of zein-PGA complex nanoparticles than that of individual zein, revealing that the combined treatments exerted a higher magnitude to modify the protein-polysaccharide complexes. It was noted that the zeta-potential of zein nanoparticles was significantly (p<0.05) decreased after the encapsulation of curcumin, which was consistent with many previous studies (Dai, Li, et al., 2018; Patel, Hu, Tiwari, & Velikov, 2010; Patel, Bouwens, & Velikov, 2010). Protein and curcumin mainly complexed through hydrogen bonds and hydrophobic interaction to form a complex. Therefore, the encapsulation and adsorption of curcumin may shield the surface charge of some amino acids, thereby reducing the zeta-potential of the particles. Patel et al. (2010) reported that as the content of curcumin increased, the zeta-potential of zein nanoparticles loaded with

curcumin continued to decrease. This result might indicate that the adsorption of excess curcumin on the surface of the particles increase the attraction between the particles and promote the aggregation of the particles.

3.2. Encapsulation efficiency and loading capacity

In order to assess the impact of different external treatments on the delivery of curcumin with the complex nanoparticles, the encapsulation efficiency (EE) and loading capacity (LC) of curcumin were determined. Among all the zein-PGA binary complex nanoparticles, ZP exhibited the highest EE of 95.33% with the highest LC of 9.58% (Fig. 2A). After HPM treatment, the EE and LC were significantly (p<0.05) decreased at 50 MPa, indicating that the extra homogenization process resulted in an inevitable loss of curcumin. With the rise in HPM pressure, the EE of curcumin in zein-PGA complex nanoparticles was continuously elevated and reached a maximum (95.29%) at 100 MPa with the LC of 9.57%. The findings revealed that HPM treatment with an appropriate pressure level facilitated the intermolecular interactions between biopolymers and curcumin, which was also reported by other researchers (Chen, Wang, Feng, Jiang, & Miao, 2019; Guo, Zhao, Chen, Chen, & Zheng, 2019). Nevertheless, the EE and LC were slightly decreased after being processed over 100 MPa. The higher pressure homogenization might cause a slight degradation of entrapped curcumin due to the rise in processing temperature generated by extrusion and friction.

The influence of thermal treatment on the EE and LC was shown in Fig. 2B. Compared to ZP-100MPa, the EE and LC of curcumin in zein-PGA complex

nanoparticles were reduced after thermal treatment. With the rise in temperature from 45 to 65 ℃, the EE in zein-PGA complex nanoparticles was decreased from 89.72% to 85.09%. Similarly, the LC of curcumin in the nanoparticles was slightly reduced from 9.01% to 8.73%. It is reasonable to assume that thermal treatment accelerated the oxidation and degradation of curcumin in the complex nanoparticles (Dai, Wei, et al., 2018a). As the temperature was elevated to 75 ℃, the EE of curcumin in zein-PGA complex nanoparticles was elevated to 92.57%. The combined HPM and thermal treatment induced the alteration of protein structure and then influenced the molecular interactions between different compounds, which altered the conformation of zein and strengthened the molecular interactions between biopolymers and curcumin (Sun, Dai, He, et al., 2016). With the rise in heating temperature, the side groups of hydrophobic aromatic amino acids were gradually exposed. During the exposure of hydrophobic amino acids, the internal structure of the complex nanoparticles was altered (Sun, Dai, Liu, et al., 2016). This result caused curcumin not only to be embedded inside the nanoparticles, but also to be adsorbed on the surface of the nanoparticles through the hydrophobic effects, thereby increasing its embedding rate. When the temperature was further elevated, an obvious declination of EE was observed in ZP-85℃,100MPa (88.41%). Therefore, the pressure of 100 MPa and temperature at 75 ℃ were confirmed to be the optimum parameters in the fabrication of curcumin loaded zein-PGA complex nanoparticles. These results proved that the coupled microfluidization and thermal treatment would have the potential to improve the EE and LC of protein-polysaccharide complex nanoparticles for delivery of nutraceuticals.

3.3. Physical stability

The physical stability of different nanoparticles was analyzed through imposing the centrifugal force. The fluctuation amplitude of the curves reflected the physical stability of the nanoparticles. As shown in Fig. 3A, ZP-50MPa exhibited the best physical stability among all the zein-PGA complex nanoparticles through HPM at different pressures. The physical stability of the complex nanoparticles was gradually reduced with HPM pressure rising. There was no obvious fluctuation in the size and zeta-potential of zein-PGA complex nanoparticles (Fig. 1). Therefore, the good stability of ZP-50MPa was mainly due to its lower content of curcumin (Fig. 2A). The encapsulation of a small quantity of curcumin could promote the molecular interactions between components (hydrophobic attraction and hydrogen bonding) to form a denser structure. Nevertheless, at the higher content of curcumin, excessive curcumin could adsorb on the particle surface and cause the particles to aggregate (A. Patel et al., 2010).

Thermal treatment showed an obvious effect on the physical stability of the complex nanoparticles (Fig. 3B). At lower temperatures, ZP-55℃,100MPa exhibited the best physical stability due to the smaller size and lower content of curcumin encapsulated. According to Brownian motion and Stokes' law, the smaller size diminished the sedimentation frequency of the nanoparticles and made them more stable (Joye et al., 2015). Additionally, the lower content of encapsulated curcumin enhanced the physical stability of the nanoparticles and contributed to the formation of compact structure with reduced interparticle hydrophobic attraction (Fig. 2B) (Dai, Li,

et al., 2018; A. R. Patel et al., 2010; Wei et al., 2018).

Fig. 3C exhibits the physical stability of different control groups. Among all the samples, Z and Z-cur were the most unstable due to their large size and strong hydrophobicity. With the external HPM and thermal treatment, the physical stability of Z-75℃, 100MPa and Z-cur-75℃, 100MPa was greatly improved. After the complexation of zein with PGA, the stability of zein-PGA complex nanoparticles became much better than that of zein nanoparticles due to the appropriate amphiphilicity and enhanced repulsion (Wei et al., 2018). Moreover, ZP-75℃, 100MPa exhibited a much better physical stability, which suggested that both HPM and thermal treatment indeed improved the physical stability of zein-PGA complexes through reducing the particle size (Fig. 1C), which was advantageous to expand their potential applications in the commercial products.

3.4. Physicochemical stability of curcumin loaded zein-PGA complex nanoparticles under environmental stresses

3.4.1. Photo stability

The photo stability of curcumin loaded in zein-PGA complex nanoparticles against UV radiation was comprehensively evaluated. Among all the samples, the curcumin encapsulated in ZP without external treatments exhibited the best chemical stability, which remained more than 50% after the exposure to UV light for 2 h (Fig. 4A). Nevertheless, the photo stability of curcumin in complex nanoparticles gradually decreased with increasing homogenization pressure. The result interpreted that the

external homogenization might alter the microstructure of the complex nanoparticles and molecular interactions between the components, thereby diminishing the chemical stability of curcumin against UV radiation.

On the contrary, thermal treatment had the opposite influence on the photo stability of curcumin entrapped in zein-PGA complex nanoparticles compared to HPM (Fig. 4B). The photo stability of curcumin in ZP-45℃, 100MPa was slightly reduced compared to that in ZP-100MPa. With the heating temperature rising, the photo stability of curcumin in zein-PGA complex nanoparticles was slightly elevated along with thermal treatment. The highest retention rate of curcumin was achieved in ZP-75℃, 100MPa after 120 min of exposure to UV light. It was noted that thermal treatment at higher temperatures could provide the complex nanoparticles with a better physical stability, which was consistent with the improved chemical stability of curcumin. It was assumed that thermal treatment influenced the microstructure of the complex nanoparticles and molecular interactions, which provided a better protection for curcumin (Dissanayake & Vasiljevic, 2009).

3.4.2. Thermal stability

The curcumin encapsulated in zein-PGA complex nanoparticles exhibited good stability after heating at 85 ℃ for 30 min with the retention rate of curcumin over 90% (Fig. 4C). Although individual thermal treatment and HPM improved thermal stability of curcumin in the complex nanoparticles, a significant decrease in the retention rate of curcumin was observed in ZP-75℃, 100MPa, showing a lack of synergistic effect between HPM and thermal treatment on enhancing the thermal stability of curcumin

loaded in zein-PGA complex nanoparticles.

The influence of thermal processing on the size (Fig. 5A) and zeta-potential (Fig. 5B) of the complex nanoparticles was investigated. A slight increase was observed in the size of zein-PGA complex nanoparticles without any external treatment, verifying that the aggregation and sedimentation occurred due to thermal processing. It was observed that HPM and thermal treatment could effectively enhance the physical stability of zein-PGA complex nanoparticles. Besides, an obvious increase appeared in the zeta-potential of all the complex nanoparticles, manifesting that the thermal processing influenced the microstructure of the nanoparticles and altered their surface properties. The enhanced thermal stability of the complex nanoparticles unraveled that HPM and heating strengthened the resistance of the nanoparticles against thermal treatment during industrial applications.

3.4.3. pH stability

The colloidal delivery systems would experience the pH fluctuation for their applications in food products. As shown in Fig. 5C and D, the size and zeta-potential of different complex nanoparticles were measured in distinct pH values. Compared to the original state (pH 4), there was a slight increase in the size of zein-PGA complex nanoparticles at pH 2. The particle size of ZP was increased from 648.3±49.8 to 707.6±54.7 nm as pH was decreased from 4 to 2, which was mainly attributed to the reduced electrostatic repulsion between the nanoparticles with a reduced absolute zeta-potential value (Wei, Yang, et al., 2020). With the coupled treatments of HPM and heating, zein-PGA complex nanoparticles remained stable under acidic condition.

When the pH was moved to 6 and 9, the size of zein-PGA complex nanoparticles was decreased significantly (p<0.05) with the rise in zeta-potential. For instance, the size of ZP was decreased to 450.2±39.8 and 372.7±21.7 nm at pH 6 and 9, respectively. The enhanced electrostatic repulsion kept the nanoparticles apart and prevented the aggregation of the nanoparticles. Compared with ZP, the associated heating and microfluidization processed complex nanoparticles kept more stable in response to pH fluctuation. As the pH was elevated from 4 to 6 and 9, the size of ZP-75℃, 100MPa was decreased from 432.8±9.6 to 388.4±11.8 and 326.2±3.6 nm.

3.4.4. Ionic strength stability

The physical stability of different complex nanoparticles was investigated under various ionic strengths (10, 50 and 100 mM). The largest increase was observed in the size of ZP with the ionic strength rising (Fig. 5E). With the external HPM and thermal treatment, the physical stability of zein-PGA complex nanoparticles was visibly improved under various ionic strengths. Meanwhile, the absolute zeta-potential value of the complex nanoparticles was gradually reduced as the ionic strength was increased through electrostatic screening (Fig. 5F). Although the electrostatic repulsion was limited, the size of zein-PGA complex nanoparticles still kept relatively stable with HPM and thermal treatment, indicating that the external processing could enhance physical stability of the nanoparticles at distinct ionic strengths.

3.5. Storage stability

To ascertain the storage stability of curcumin loaded zein-PGA complex

nanoparticles, different samples were stored for one week at 4, 37, and 55 ℃. After storage, the size of zein-PGA complex nanoparticles was increased to different magnitudes (Fig. 6A). Interestingly, the largest increase in the particle size was observed in the complex nanoparticles stored at 4 ℃, which was larger than those stored at 37 ℃ and 55 ℃. Besides, it was noticed that the absolute zeta-potential value of the nanoparticles was increased with the storage temperature rising, thereby providing the sufficient electrostatic repulsion to keep the nanoparticles apart during storage period (Fig. 6B), which might be attributed to the thermal degradation of curcumin (Dai, Wei, et al., 2018b).

Fig. 6C shows the retention rate of curcumin encapsulated in zein-PGA complex nanoparticles stored at different temperatures. It was clearly noted that the retention rate of curcumin in the nanoparticles decreased with the storage temperature rising, revealing that the higher temperature accelerated the chemical degradation of curcumin. In terms of the storage stability of different nanoparticles, all the samples exhibited the excellent protection of curcumin at 4 ℃ without significant differences. As the temperature was elevated to 37 ℃, ZP-75℃ showed the best chemical stability of curcumin among zein-PGA complex nanoparticles. When the nanoparticles were stored at 55 ℃, no obvious difference was found in zein-PGA complex nanoparticles. Nevertheless, the coupled treatment of HPM and heating provided a better protection for curcumin in the complex nanoparticles compared to individual HPM or thermal treatment. As discussed above, the size and zeta-potential of the complex nanoparticles seemed to be correlated with the thermal degradation of curcumin. The thermal

degradation of curcumin promoted the increase in absolute zeta-potential value and the decrease in particle size (Fig. 6A and B), which was mainly ascribed to alteration of the particle structure and molecular interactions. The degradation of curcumin caused by the temperature rise weakened the hydrophobic interaction between the particles and reduced the interparticle attraction. On the other hand, the rise in zeta-potential increased the electrostatic repulsion between the particles, causing the particles to separate from each other. These results testified that the combined HPM and thermal treatment could extend the shelf-life of nanoparticle-based delivery vehicles.

3.6. Fluorescence property

Fluorescence is utilized to investigate the alteration in the polarity of surrounding environment of fluorophore (Wei, Yu, et al., 2019), which can be utilized to assess the molecular interactions between biopolymers and curcumin. As shown in Fig. 7, zein exhibited a fluorescence emission peak at 304 nm after being excited at 280 nm, which was attributed to its high proportion of tyrosine residues (Sun et al., 2017c; Wei et al., 2018). Upon the encapsulation of curcumin, the tyrosine fluorescence got almost quenched and the fluorescence intensity of Z-cur was greatly reduced, which was consistent with the complexation of other proteins and polyphenols (Dai, Wei, et al., 2018a; Joye et al., 2015; Liang, Tajmir-Riahi, & Subirade, 2008). Nevertheless, the complexation of zein with PGA increased the fluorescence intensity of zein, indicating a more apolar micro-environment of tyrosine residues (Wei et al., 2018). After HPM at different pressures, the fluorescence intensity of the protein was decreased greatly,

which was consistent with the reports from other researchers (Fig. 7A) (Chen et al., 2019; Sun, Yang, et al., 2016). The decreased fluorescence intensity might be ascribed to the entanglement and aggregation of molecular chains generated by shear, impact and vibration at a specific pressure (Dissanayake & Vasiljevic, 2009; O'Sullivan, Arellano, Pichot, & Norton, 2014). In zein-PGA complex nanoparticles, most of aromatic amino acids that could produce fluorescence were inside the zein molecule, and the locally environmental polarity was less than that of the aqueous solution for the nanoparticles. During the denaturation of zein, the side chain groups of aromatic amino acid molecules were gradually exposed, and the increased environmental polarity of amino acid molecules resulted in a decrease in fluorescence intensity (Liang et al., 2008).

The thermal treatment also decreased the fluorescence intensity of zein slightly with the rise in the heating temperature (Fig. 7B). During thermal processing, the conformation of zein underwent some changes, which exposed the amino acid residues buried inside the native structure, leading to a decrease in the fluorescence intensity (Sun, Dai, He, et al., 2016). However, in control groups, the external processing of HPM and heat exhibited much less influence on zein-PGA complex nanoparticles in the absence of curcumin (Fig. 7C). The fluorescence intensity of zein in Z-P was decreased slightly during the coupled treatment of HPM and heating. The phenomenon testified that the structure of the complex nanoparticles was very stable without curcumin. The incorporation of PGA indeed provided an effective protection for the conformation of zein during external processing (Sun, Dai, He, et al., 2016; Sun, Yang, et al., 2016).

3.7. Circular dichroism

The alterations in CD signals are easily assigned to distinct structural features of proteins. The different types of regular secondary structure found in proteins give rise to characteristic CD spectra in the far UV (Kelly, Jess, & Price, 2005). The secondary structure of zein was calculated by CD in the far-UV range (260–190 nm) by SELCON 3 on an online server DICHROWEB (Fig. 8). The secondary structure of zein contained more than 50% α-helix (Wei et al., 2018). It was noted that the process of emulsification-evaporation decreased the content of α-helix and then increased the content of β-sheet accordingly (Selling et al., 2007), revealing the disorder-to-order state of secondary structure (Dyson & Wright, 2005).

The α-helix content of zein was greatly increased from 11.9% (zein colloidal particles) to 43.7% (ZP), indicating that the α-helix structure in zein-PGA complex nanoparticles was effectively protected (Fig. 8A). Nevertheless, HPM treatment at the pressure of 50 MPa led to a dramatic decrease of α-helix fraction from 44.3% to 16.0% and an increase of β-sheet fraction from 13.1% to 32.5% in zein-PGA complex nanoparticles. The results revealed that HPM induced the unfolding and aggregation of proteins, and promoted the transition from α-helix to β-sheet in the secondary structure of zein. The HPM-induced intermolecular β-sheet aggregation enhanced the microstructural stability of the nanoparticles, which was consistent with the decreased fluorescence intensity (Sun, Wei, Li, Dai, & Gao, 2017b; Wei, Yu, et al., 2019). With the increase in the pressure from 50 to 150 MPa, there was a slight increase in α-helix

fraction of zein-PGA complex nanoparticles (Fig. 8B), manifesting that structural rearrangement of zein molecules was generated by microfluidization at the higher pressure (Sun, Dai, Liu, et al., 2016).

Thermal treatment of zein-PGA complex nanoparticles resulted in a slight increase in α-helix fraction and a decrease in β-sheet fraction (Fig. 8C), which verified the hypothesis that zein molecular chains were partially unfolded due to thermal treatment. Compared with single HPM, the coupled treatment of HPM and heating showed different impacts on modulating the secondary structure of zein, especially at 55 ℃. The results clearly revealed that HPM had a more significant effect on the conformational change of zein compared to thermal treatment, which was consistent with the fluorescence intensity of zein.

3.8. FTIR

FTIR technique is a versatile tool to monitor change in the functional groups of biopolymers and analyze the intermolecular interactions between zein, PGA and curcumin during the formation of the complex nanoparticles (Fig. 9A). Two major characteristic peaks of zein were observed at around 1658.1 and 1540.7 cm^{-1}, which were indicatives of the amide I band (1750-1600 cm^{-1}) and amide II band (1550-1510 cm^{-1}). An absorption band of O-H stretching was found at 3311.2 cm^{-1}. The curcumin spectrum showed characteristics peaks at 1602.0, 1583.1, 1512.1, 1455.7, 1375.2, and 963.4 cm^{-1}, probably due to aromatic -C=C- stretching, olefinic -C-C- stretching, aromatic ring C=C- stretching, aromatic ring -C=C- stretching, -C-O- stretching

vibration, and trans olefinic -C=C- stretching, respectively (Dai, Wei, et al., 2018b; Fan et al., 2018). After the complexation of zein with PGA, the intensity of absorption peak corresponding to hydrogen bonds and amide II band was obviously increased. This was attributed to the intermolecular hydrogen bonding and electrostatic interaction, which mainly contributed to the formation of zein-PGA complex nanoparticles.

The influence of HPM pressure on the structure and molecular interactions of zein-PGA complex nanoparticles was demonstrated in Fig. 9B. With the homogenizing pressure increasing, the intensity of absorbance peaks at around 1660 and 3310 cm^{-1} was continuously elevated due to the formation of β-sheet aggregates through intermolecular hydrogen bonding. The conformational change of the protein has been confirmed by the fluorescence intensity and circular dichroism. During thermal treatment, the intensity of absorption peaks corresponding to amide band I and hydrogen bonding was slightly decreased with the rise in heating temperature, which meant that thermal treatment promoted the transition from β-sheet into α-helix and interrupted the intermolecular hydrogen bonding (Fig. 9C). Besides, the reduction of β-sheet regions at the interface of proteins was related to the conformational freedom in the protein structure and aggregation of the particles (Lefèvre, Subirade, & Pézolet, 2005; Mangavel, Barbot, Popineau, & Guéguen, 2001).

3.9. X-ray diffraction

Fig. 10 showed the crystalline diffraction patterns of pure curcumin, zein, PGA, and zein-PGA complex particles. For individual biopolymers, zein and PGA had

relatively flat peaks, which interpreted the amorphous nature of biopolymers (Fig. 10A). On the contrary, pure curcumin was highly crystallized with characteristic sharp diffraction peaks. Nevertheless, there were no obvious diffraction peaks belonging to curcumin after its encapsulation into zein-PGA binary complex nanoparticles with an amorphous state. Compared to individual zein and PGA, the diffraction peaks of zein-PGA complex nanoparticles at previous angles further decreased and even disappeared, interpreting that the intermolecular interactions among individual components altered the physical state in the formation of the complex nanoparticles (Sun et al., 2017b).

The different homogenization pressures could scarcely exhibit the obvious influence on the XRD spectra of zein-PGA complex nanoparticles in an amorphous state (Fig. 10B). The thermal treatment showed different effects on the molecular structure of the complex nanoparticles. Among zein-PGA complex nanoparticles, the diffraction intensity of the nanoparticles was increased firstly and then decreased with the heating temperature rising (Fig. 10B). The findings were attributed to distinct microstructures of the complex nanoparticles induced by different heating temperatures (Dai, Wei, et al., 2018b; Wei, Zhang, et al., 2019). As evidenced by circular dichroism, in the secondary structure of zein, the proportion of α-helix was reduced and the fraction of β-helix was increased progressively when the temperature was elevated from 65 to 85 ℃.

3.10. Morphology

The morphological features of the complex nanoparticles were observed with the

aid of FE-SEM. As shown in Fig. 11, ZP without curcumin entrapped exhibited a regular shape with the rough surface, which was difficult to distinguish individual nanoparticles. The connection among the nanoparticles was provided by excessive PGA adsorbed on the surface of complex nanoparticles as interparticle bridges (Wei et al., 2018). After the coupled treatments of HPM and heating, the long molecular chains of PGA could fold and interact fully with zein molecules, thereby forming spherical complex nanoparticles. Interestingly, after the encapsulation of curcumin, ZP exhibited a more uniform size distribution, which might be because the curcumin entrapped enhanced the hydrophobic effect inside the nanoparticles, thus forming a denser structure. With the combined HPM and heating, the size of ZP-75℃,100MPa was visibly reduced, but partial aggregation of the nanoparticles occurred (Sun, Dai, Liu, et al., 2016). The phenomenon was reasonably attributable to the enhanced hydrophobic attraction between the nanoparticles due to the external treatment.

3.11. In vitro gastrointestinal digestion

The digestion behavior of curcumin loaded complex nanoparticles was investigated in the simulated GI tract. The size of the nanoparticles during *in vitro* digestion was dependent on the digestion time in the simulated GI tract. As shown in Fig. 12A, the particle size kept stable or even decreased slightly after exposure to the gastric phase. The phenomenon was consistent with our previous study, which reported the digestion fate of β-carotene loaded zein-PGA nanoparticles (Wei et al., 2018). The result implied that zein-PGA complex nanoparticles exhibited a better stability in the

stomach phase against pepsin. There was a stepwise increase in the size of curcumin loaded complex nanoparticles after exposure to the small intestine phase, revealing that the structure of the complex nanoparticles was gradually broken down in the small intestine.

The release percentages of curcumin in the complex nanoparticles at 30, 60, 90, 120, 150- and 180-min during GIT are shown in Fig. 12B. The lowest release percentage (11.43 ± 0.97%) of curcumin in the gastric phase was obtained in zein-PGA complex nanoparticles without any external processing. After HPM processing at different pressures, the shear, impact and vibration within microfluidization caused the entanglement and aggregation of molecular chains in zein. In zein-PGA complex nanoparticles, the side chain groups of aromatic amino acid molecules were gradually exposed, the internal structure of the complex nanoparticles was altered, and the hydrophobic interaction between curcumin and zein was destroyed, promoting the release of curcumin from the nanoparticles in the gastric phase. After thermal treatment, the conformation of zein underwent an obvious alteration, which also exposed the amino acid residues buried inside the native structure, thus slightly facilitating the release of curcumin from zein-PGA complex nanoparticles.

After being digested for 180 min, most of curcumin in the complex nanoparticles was released in the intestine, especially at initial 30 min. Among zein-PGA complex nanoparticles, ZP-75℃ showed the highest release percentage of curcumin (98.95 ± 0.24%) in the intestine phase. Additionally, ZP-75℃, 100MPa exhibited the lowest release percentage (81.93 ± 0.74%) after the coupled treatments of HPM and heating.

The results revealed that zein-PGA complex nanoparticles without any external processing showed the highest release percentage of curcumin due to their looser structure, thereby accelerating the release of curcumin in the gastric phase.

Different from the release percentage of curcumin, ZP exhibited the lowest bioaccessibility (12.31 ± 0.64%) (Fig. 12C). With individual HPM or thermal treatment, the bioaccessibility of curcumin was slightly improved compared to ZP. After the coupled treatments of HPM and heating, the curcumin bioaccessibility was significantly (p<0.05) elevated to a higher level (52.35 ± 1.58%) in ZP-75℃,100MPa. Although individual HPM or thermal treatment could enhance the bioaccessibility of curcumin during *in vitro* digestion, the HPM and thermal treatment exhibited a greater effect on enhancing the bioaccessibility of curcumin, and even its bioaccessibility was higher than the sum of bioaccessibility of curcumin loaded in the nanoparticles with two individual treatments. Therefore, HPM and heat treatment showed not only a simple additive effect, but a synergistic effect on enhancing the bioaccessibility of curcumin. The more uniform size and compact structure promoted to elevate significantly ($p < 0.05$) the bioaccessibility of curcumin in the small intestine phase from zein-PGA complex nanoparticles, which might increase the adsorption of bile salts and digestive enzyme onto the nanoparticle surface. The strengthened interactions between the complex nanoparticles and SIF enhanced the release of curcumin and formation of mixed micelles (Fan et al., 2018).

The FE-SEM images revealed that the morphology of the complex nanoparticles almost kept stable after simulated gastric digestion (Fig. 12D), which was dominantly

ascribed to the resistance of zein against pepsin in the gastric phase (A. R. Patel & Velikov, 2014; Penalva et al., 2015; Wei et al., 2018). After exposure to the small intestine phase for 120 min, zein-PGA complex nanoparticles were collapsed in shape and agglomerated. The digestion of zein by pancreatin led to a distorted shape and more release of curcumin. The aggregation of zein-PGA complex nanoparticles obviously occurred in the intestinal phase, thereby limiting the release percentage and bioaccessibility of curcumin in the nanoparticles during the intestinal digestion.

4. Conclusion

In the present study, the microfluidization pressure at 100 MPa and heating temperature at 75 ℃ were the optimum parameters for providing a better protection of curcumin entrapped in zein-PGA complex nanoparticles. With the treatment of HPM, the complex nanoparticles exhibited a better stability under various environmental stresses (pH, ionic strength, light and heat) and storage conditions (37 and 55 ℃). Nevertheless, compared with single HPM treatment, the combined HPM and thermal treatment did not show a significant advantage in improving the stability and functional properties of the complex nanoparticles. Through the observation of FE-SEM, HPM and thermal treatment facilitated the formation of zein-PGA complex nanoparticles with a more uniform size and spherical shape. *In vitro* digestion model revealed that the complex nanoparticles exhibited the excellent gastric stability and sustained-release of curcumin in the small intestine phase. Notablely, the bioaccessibility of curcumin was enhanced after the coupled treatment of HPM and heating. The findings from this

study confirmed that HPM alone could effectively enhance the functional attributes, environmental stability, and sustained-release of curcumin-loaded protein-polysaccharide complex nanoparticles. A new insight into the potential application of HPM and heating is provided in the design and development of nanoparticle-based delivery vehicles.

Corresponding Author

*E-mail: gyxcau@126.com

Notes

The authors declare no competing financial interest.

Acknowledgement

Financial support from the National Natural Science Foundation of China (No.31871842) is gratefully acknowledged. We acknowledge Jianhui Li from the Institute of Biophysics, China Academy of Sciences, for performing the circular dichroism analysis.

References:

Chen, G., Wang, S., Feng, B., Jiang, B., & Miao, M. (2019). Interaction between soybean protein and tea polyphenols under high pressure. *Food Chemistry*, *277*(November 2018), 632–638. https://doi.org/10.1016/j.foodchem.2018.11.024

Dai, L., Li, R., Wei, Y., Sun, C., Mao, L., & Gao, Y. (2018). Fabrication of zein and rhamnolipid complex nanoparticles to enhance the stability and in vitro release of curcumin. *Food Hydrocolloids*, *77*, 617–628.

https://doi.org/10.1016/j.foodhyd.2017.11.003

Dai, L., Sun, C., Li, R., Mao, L., Liu, F., & Gao, Y. (2017). Structural characterization, formation mechanism and stability of curcumin in zein-lecithin composite nanoparticles fabricated by antisolvent co-precipitation. *Food Chemistry*, *237*, 1163–1171. https://doi.org/10.1016/j.foodchem.2017.05.134

Dai, L., Wei, Y., Sun, C., Mao, L., McClements, D. J., & Gao, Y. (2018a). Development of protein-polysaccharide-surfactant ternary complex particles as delivery vehicles for curcumin. *Food Hydrocolloids*, *85*(17), 75–85. https://doi.org/10.1016/j.foodhyd.2018.06.052

Dai, L., Wei, Y., Sun, C., Mao, L., McClements, D. J., & Gao, Y. (2018b). Development of protein-polysaccharide-surfactant ternary complex particles as delivery vehicles for curcumin. *Food Hydrocolloids*, *85*(17), 75–85. https://doi.org/10.1016/j.foodhyd.2018.06.052

Dissanayake, M., & Vasiljevic, T. (2009). Functional properties of whey proteins affected by heat treatment and hydrodynamic high-pressure shearing. *Journal of Dairy Science*, *92*(4), 1387–1397. https://doi.org/10.3168/jds.2008-1791

Dyson, H. J., & Wright, P. E. (2005). Intrinsically unstructured proteins and their functions. *Nature Reviews Molecular Cell Biology*, *6*(3), 197–208. https://doi.org/10.1038/nrm1589

Fan, Y., Liu, Y., Gao, L., Zhang, Y., & Yi, J. (2018). Improved chemical stability and cellular antioxidant activity of resveratrol in zein nanoparticle with bovine serum albumin-caffeic acid conjugate. *Food Chemistry*, *261*, 283–291.

https://doi.org/10.1016/J.FOODCHEM.2018.04.055

Guo, Z., Zhao, B., Chen, J., Chen, L., & Zheng, B. (2019). Insight into the characterization and digestion of lotus seed starch-tea polyphenol complexes prepared under high hydrostatic pressure. *Food Chemistry*, *297*(March). https://doi.org/10.1016/j.foodchem.2019.124992

Hu, X., Zhao, M., Sun, W., Zhao, G., & Ren, J. (2011). Effects of microfluidization treatment and transglutaminase cross-linking on physicochemical, functional, and conformational properties of peanut protein isolate. *Journal of Agricultural and Food Chemistry*, *59*(16), 8886–8894. https://doi.org/10.1021/jf201781z

Huang, X., Dai, Y., Cai, J., Zhong, N., Xiao, H., McClements, D. J., & Hu, K. (2017). Resveratrol encapsulation in core-shell biopolymer nanoparticles: Impact on antioxidant and anticancer activities. *Food Hydrocolloids*, *64*, 157–165. https://doi.org/10.1016/j.foodhyd.2016.10.029

Joye, I. J., Davidov-Pardo, G., & McClements, D. J. (2015). Encapsulation of resveratrol in biopolymer particles produced using liquid antisolvent precipitation. Part 2: Stability and functionality. *Food Hydrocolloids*, *49*, 127–134. https://doi.org/10.1016/j.foodhyd.2015.02.038

Kelly, S. M., Jess, T. J., & Price, N. C. (2005). How to study proteins by circular dichroism. *Biochimica et Biophysica Acta - Proteins and Proteomics*, *1751*(2), 119–139. https://doi.org/10.1016/j.bbapap.2005.06.005

Kim, S., & Xu, J. (2008). Aggregate formation of zein and its structural inversion in aqueous ethanol. *Journal of Cereal Science*, *47*(1), 1–5.

https://doi.org/10.1016/j.jcs.2007.08.004

Lefèvre, T., Subirade, M., & Pézolet, M. (2005). Molecular description of the formation and structure of plasticized globular protein films. *Biomacromolecules*, *6*(6), 3209–3219. https://doi.org/10.1021/bm050540u

Liang, L., Tajmir-Riahi, H. A., & Subirade, M. (2008). Interaction of β-Lactoglobulin with resveratrol and its biological implications. *Biomacromolecules*, *9*(1), 50–56. https://doi.org/10.1021/bm700728k

Mangavel, C., Barbot, J., Popineau, Y., & Guéguen, J. (2001). Evolution of wheat gliadins conformation during film formation: A Fourier transform infrared study. *Journal of Agricultural and Food Chemistry*, *49*(2), 867–872. https://doi.org/10.1021/jf0009899

McClements, D. J., & Gumus, C. E. (2016). Natural emulsifiers — Biosurfactants, phospholipids, biopolymers, and colloidal particles: Molecular and physicochemical basis of functional performance. *Advances in Colloid and Interface Science*, *234*, 3–26. https://doi.org/10.1016/j.cis.2016.03.002

Minekus, M., Alminger, M., Alvito, P., Ballance, S., Bohn, T., Bourlieu, C., … Brodkorb, A. (2014). A standardised static in vitro digestion method suitable for food-an international consensus. *Food and Function*, *5*(6), 1113–1124. https://doi.org/10.1039/c3fo60702j

Momany, F. A., Sessa, D. J., Lawton, J. W., Selling, G. W., Hamaker, S. A. H., & Willett, J. L. (2006). Structural characterization of α-zein. *Journal of Agricultural and Food Chemistry*, *54*(2), 543–547. https://doi.org/10.1021/jf058135h

O'Sullivan, J., Arellano, M., Pichot, R., & Norton, I. (2014). The effect of ultrasound treatment on the structural, physical and emulsifying properties of dairy proteins. *Food Hydrocolloids*, *42*, 386–396. https://doi.org/10.1016/J.FOODHYD.2014.05.011

Paliwal, R., & Palakurthi, S. (2014). Zein in controlled drug delivery and tissue engineering. *Journal of Controlled Release*, *189*, 108–122. https://doi.org/10.1016/J.JCONREL.2014.06.036

Patel, A., Hu, Y., Tiwari, J. K., & Velikov, K. P. (2010). Synthesis and characterisation of zein-curcumin colloidal particles. *Soft Matter*, *6*(24), 6192–6199. https://doi.org/10.1039/c0sm00800a

Patel, A. R., Bouwens, E. C. M., & Velikov, K. P. (2010). Sodium caseinate stabilized zein colloidal particles. *Journal of Agricultural and Food Chemistry*, *58*(23), 12497–12503. https://doi.org/10.1021/jf102959b

Patel, A. R., & Velikov, K. P. (2014). Zein as a source of functional colloidal nano- and microstructures. *Current Opinion in Colloid and Interface Science*, *19*(5), 450–458. https://doi.org/10.1016/j.cocis.2014.08.001

Penalva, R., Esparza, I., Larraneta, E., González-Navarro, C. J., Gamazo, C., & Irache, J. M. (2015). Zein-Based Nanoparticles Improve the Oral Bioavailability of Resveratrol and Its Anti-inflammatory Effects in a Mouse Model of Endotoxic Shock. *Journal of Agricultural and Food Chemistry*, *63*(23), 5603–5611. https://doi.org/10.1021/jf505694e

Selling, G. W., Hamaker, S. A. H., & Sessa, D. J. (2007). Effect of solvent and

temperature on secondary and tertiary structure of zein by circular dichroism. *Cereal Chemistry*, *84*(3), 265–270. https://doi.org/10.1094/CCHEM-84-3-0265

Semenova, M. (2017). Protein–polysaccharide associative interactions in the design of tailor-made colloidal particles. *Current Opinion in Colloid and Interface Science*, *28*, 15–21. https://doi.org/10.1016/j.cocis.2016.12.003

Shukla, R., & Cheryan, M. (2001). Zein: The industrial protein from corn. *Industrial Crops and Products*, *13*(3), 171–192. https://doi.org/10.1016/S0926-6690(00)00064-9

Sobisch, T., & Lerche, D. (2008). Thickener performance traced by multisample analytical centrifugation. *Colloids and Surfaces A: Physicochemical and Engineering Aspects*, *331*(1–2), 114–118. https://doi.org/10.1016/J.COLSURFA.2008.05.040

Song, X., Zhou, C., Fu, F., Chen, Z., & Wu, Q. (2013). Effect of high-pressure homogenization on particle size and film properties of soy protein isolate. *Industrial Crops and Products*, *43*(1), 538–544. https://doi.org/10.1016/j.indcrop.2012.08.005

Sun, C., Dai, L., He, X., Liu, F., Yuan, F., & Gao, Y. (2016). Effect of heat treatment on physical, structural, thermal and morphological characteristics of zein in ethanol-water solution. *Food Hydrocolloids*, *58*, 11–19. https://doi.org/10.1016/j.foodhyd.2016.02.014

Sun, C., Dai, L., Liu, F., & Gao, Y. (2016). Simultaneous treatment of heat and high pressure homogenization of zein in ethanol-water solution: Physical, structural,

thermal and morphological characteristics. *Innovative Food Science and Emerging Technologies*, *34*, 161–170. https://doi.org/10.1016/j.ifset.2016.01.016

Sun, C., Wei, Y., Li, R., Dai, L., & Gao, Y. (2017a). Quercetagetin-Loaded Zein-Propylene Glycol Alginate Ternary Composite Particles Induced by Calcium Ions: Structure Characterization and Formation Mechanism. *Journal of Agricultural and Food Chemistry*, *65*(19), 3934–3945. https://doi.org/10.1021/acs.jafc.7b00921

Sun, C., Wei, Y., Li, R., Dai, L., & Gao, Y. (2017b). Quercetagetin-Loaded Zein-Propylene Glycol Alginate Ternary Composite Particles Induced by Calcium Ions: Structure Characterization and Formation Mechanism. *Journal of Agricultural and Food Chemistry*, *65*(19), 3934–3945. https://doi.org/10.1021/acs.jafc.7b00921

Sun, C., Wei, Y., Li, R., Dai, L., & Gao, Y. (2017c). Quercetagetin-Loaded Zein–Propylene Glycol Alginate Ternary Composite Particles Induced by Calcium Ions: Structure Characterization and Formation Mechanism. *Journal of Agricultural and Food Chemistry*, *65*(19), 3934–3945. https://doi.org/10.1021/acs.jafc.7b00921

Sun, C., Yang, J., Liu, F., Yang, W., Yuan, F., & Gao, Y. (2016). Effects of Dynamic High-Pressure Microfluidization Treatment and the Presence of Quercetagetin on the Physical, Structural, Thermal, and Morphological Characteristics of Zein Nanoparticles. *Food and Bioprocess Technology*, *9*(2), 320–330. https://doi.org/10.1007/s11947-015-1627-4

Wei, Y., Sun, C., Dai, L., Zhan, X., & Gao, Y. (2018). Structure, physicochemical stability and in vitro simulated gastrointestinal digestion properties of β-carotene loaded zein-propylene glycol alginate composite nanoparticles fabricated by emulsification-evaporation method. *Food Hydrocolloids*, *81*, 149–158. https://doi.org/10.1016/j.foodhyd.2018.02.042

Wei, Y., Yang, S., Zhang, L., Dai, L., Tai, K., Liu, J., … Mackie, A. (2020). Fabrication, characterization and in vitro digestion of food grade complex nanoparticles for co-delivery of resveratrol and coenzyme Q10. *Food Hydrocolloids*, *105*(17), 105791. https://doi.org/10.1016/J.FOODHYD.2020.105791

Wei, Y., Yu, Z., Lin, K., Sun, C., Dai, L., Yang, S., … Gao, Y. (2019). Fabrication and characterization of resveratrol loaded zein-propylene glycol alginate-rhamnolipid composite nanoparticles: Physicochemical stability, formation mechanism and in vitro digestion. *Food Hydrocolloids*, *95*, 336–348. https://doi.org/10.1016/j.foodhyd.2019.04.048

Wei, Y., Yu, Z., Lin, K., Yang, S., Tai, K., Liu, J., … Gao, Y. (2020). Fabrication, Physicochemical Stability and Microstructure of Coenzyme Q10 Pickering Emulsions Stabilized by Resveratrol Loaded Composite Nanoparticles. *Journal of Agricultural and Food Chemistry*, *0*(ja). https://doi.org/10.1021/acs.jafc.9b06678

Wei, Y., Zhang, L., Yu, Z., Lin, K., Yang, S., Dai, L., … Gao, Y. (2019). Enhanced stability, structural characterization and simulated gastrointestinal digestion of coenzyme Q10 loaded ternary nanoparticles. *Food Hydrocolloids*, *94*, 333–344. https://doi.org/10.1016/j.foodhyd.2019.03.024

Yao, M., Xiao, H., & McClements, D. J. (2014). Delivery of Lipophilic Bioactives: Assembly, Disassembly, and Reassembly of Lipid Nanoparticles. *Annual Review of Food Science and Technology*, *5*(1), 53–81. https://doi.org/10.1146/annurev-food-072913-100350

Ye, R., & Harte, F. (2014). High pressure homogenization to improve the stability of casein-hydroxypropyl cellulose aqueous systems. *Food Hydrocolloids*, *35*, 670–677. https://doi.org/10.1016/j.foodhyd.2013.08.022

Zhang, B., Luo, Y., & Wang, Q. (2011). Effect of acid and base treatments on structural, rheological, and antioxidant properties of α-zein. *Food Chemistry*, *124*(1), 210–220. https://doi.org/10.1016/j.foodchem.2010.06.019

Zhong, J., Tu, Y., Liu, W., Xu, Y., Liu, C., & Dun, R. (2014). Antigenicity and conformational changes of β-lactoglobulin by dynamic high pressure microfluidization combining with glycation treatment. *Journal of Dairy Science*, *97*(8), 4695–4702. https://doi.org/10.3168/jds.2013-7829

Figure captions

Fig. 1 Effects of individual microfludization pressure (A) and heating temperature (B) on the size and zeta-potential of curcumin loaded zein-PGA complex nanoparticles; effects of combined heating temperature and microfludization pressure on the size and zeta-potential of individual and complex nanoparticles in the control group (C). (Different superscript letters (A, B, C…and a,b,c…) in the figure indicate significant differences ($p < 0.05$) in the particle size and zeta-potential)

Fig. 2 Impact of microfludization pressure on the EE and LC of curcumin loaded in zein-PGA complex nanoparticles (A); impact of heating temperature on the EE and LC of curcumin loaded in zein-PGA complex nanoparticles (B); (Different superscript letters (A, B, C…) in the figure indicate significant differences ($p < 0.05$))

Fig. 3 Influence of microfludization pressure on the physical stability of curcumin loaded zein-PGA complex nanoparticles (A); influence of heating temperature on the physical stability of curcumin loaded zein-PGA complex nanoparticles (B); the physical stability of the nanoparticles in the control group (C);

Fig. 4 Influence of microfludization pressure (A) and heating temperature (B) on the photo stability of curcumin loaded in zein-PGA complex nanoparticles; the thermal stability of curcumin loaded in zein-PGA complex nanoparticles (C);

Fig. 5 Effects of thermal treatment, pH and ionic strength on the particle size (A, C and E) and zeta-potential (B, D and F) of curcumin loaded zein-PGA complex nanoparticles; (Different superscript letters (A, B, C…) in the figure indicate

significant differences ($p < 0.05$))

Fig. 6 Effect of different storage temperatures on the size (A) and zeta-potential (B) of curcumin loaded zein-PGA complex nanoparticles; the retention rate of curcumin loaded in zein-PGA complex nanoparticles at different storage temperatures (C); (Different superscript letters (A, B, C…) in the figure indicate significant differences ($p < 0.05$))

Fig. 7 Effects of microfludization pressure (A) and heating temperature (B) on the fluorescence property of curcumin loaded zein-PGA complex nanoparticles; the fluorescence property of the nanoparticles in the control group (C);

Fig. 8 Circular dichroism of individual and complex nanoparticles in the control group (A); effects of microfludization pressure (B) and heating temperature (C) on the circular dichroism of curcumin loaded zein-PGA complex nanoparticles;

Fig. 9 FTIR spectra of individual and complex nanoparticles in the control group (A); effects of microfludization pressure (B) and heating temperature (C) on the FTIR spectra of zein-PGA complex nanoparticles;

Fig. 10 XRD spectra of individual component and nanoparticles in the control group (A); effects of microfludization pressures (B) and heating temperatures (C) on the XRD spectra of zein-PGA complex nanoparticles;

Fig. 11 SEM images of curcumin loaded zein-PGA complex nanoparticles with and without individual microfludization and heating or their combined treatments;

Fig. 12 The fluctuation in the mean size of curcumin loaded zein-PGA complex nanoparticles (A) and release percentage of curcumin in zein-PGA complex nanoparticles (B) during *in vitro* digestion; the bioaccessibility of curcumin loaded in different complex nanoparticles (C) and the morphology of different complex

nanoparticles during *in vitro* digestion (D). (Different superscript letters (A, B, C…) in the figure indicate significant differences ($p < 0.05$))

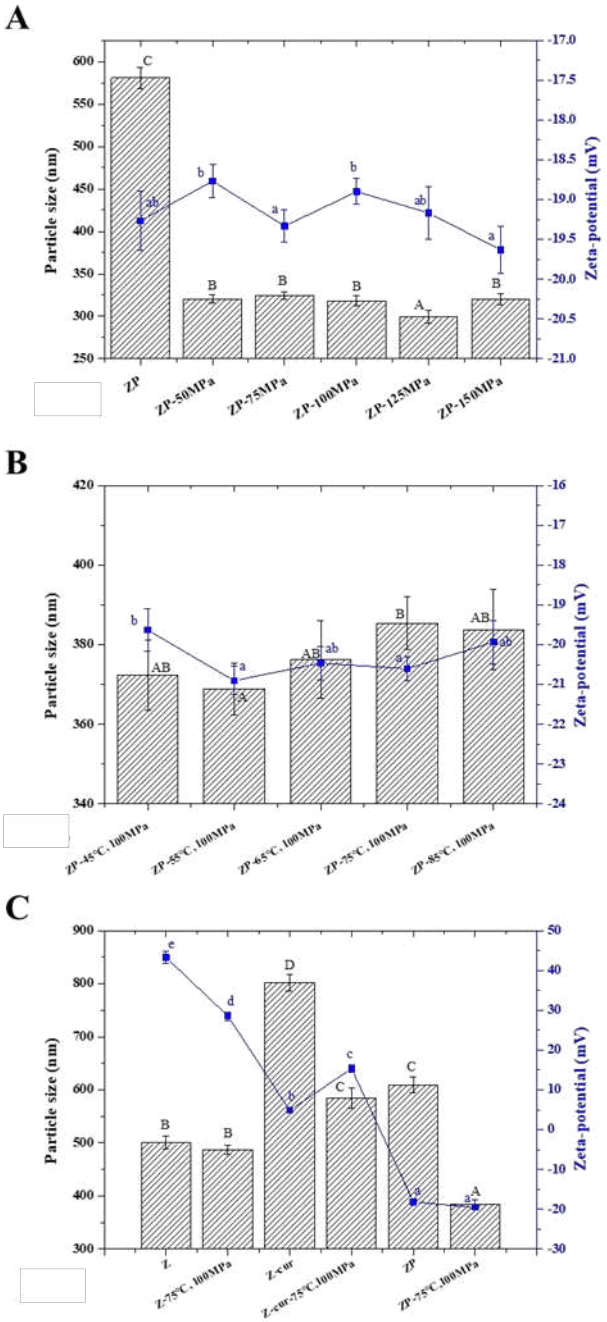

Fig. 1

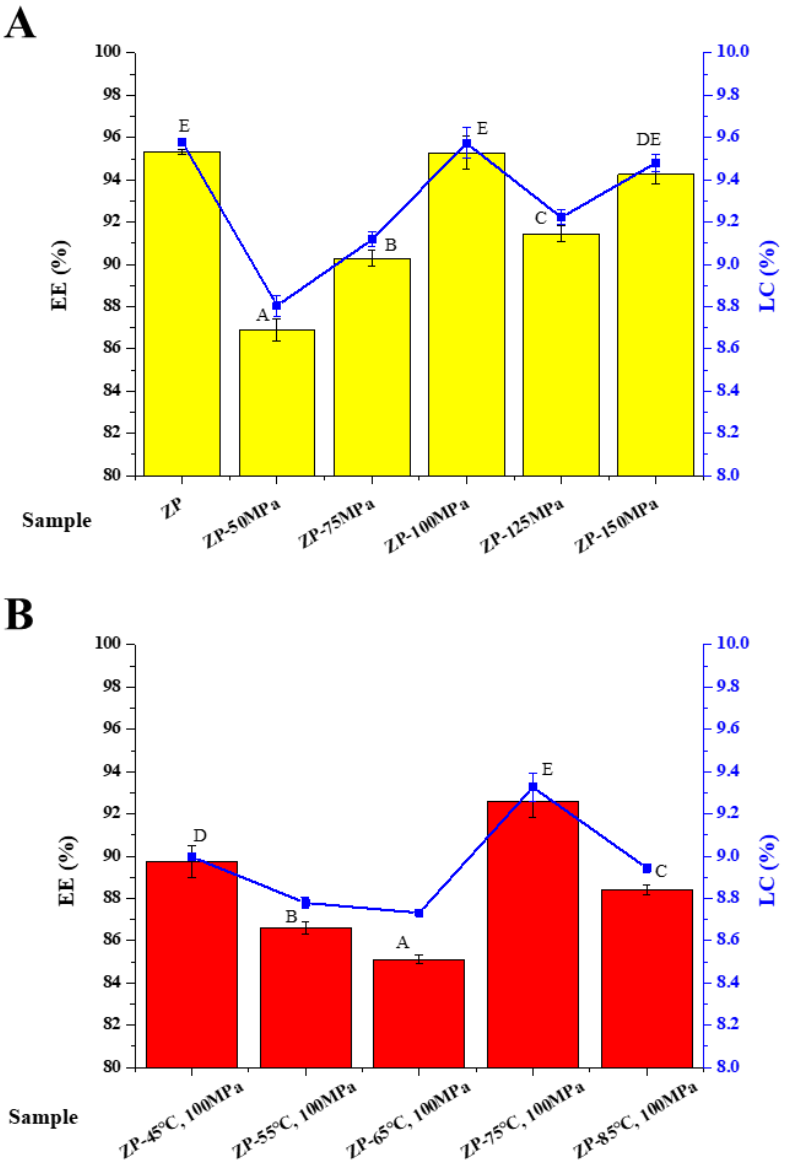
A
EE (%)
LC (%)
Sample
ZP
ZP-50MPa
ZP-75MPa
ZP-100MPa
ZP-125MPa
ZP-150MPa
E
A
B
E
C
DE
B
D
B
A
E
C
ZP-45°C, 100MPa
ZP-55°C, 100MPa
ZP-65°C, 100MPa
ZP-75°C, 100MPa
ZP-85°C, 100MPa

Fig. 2

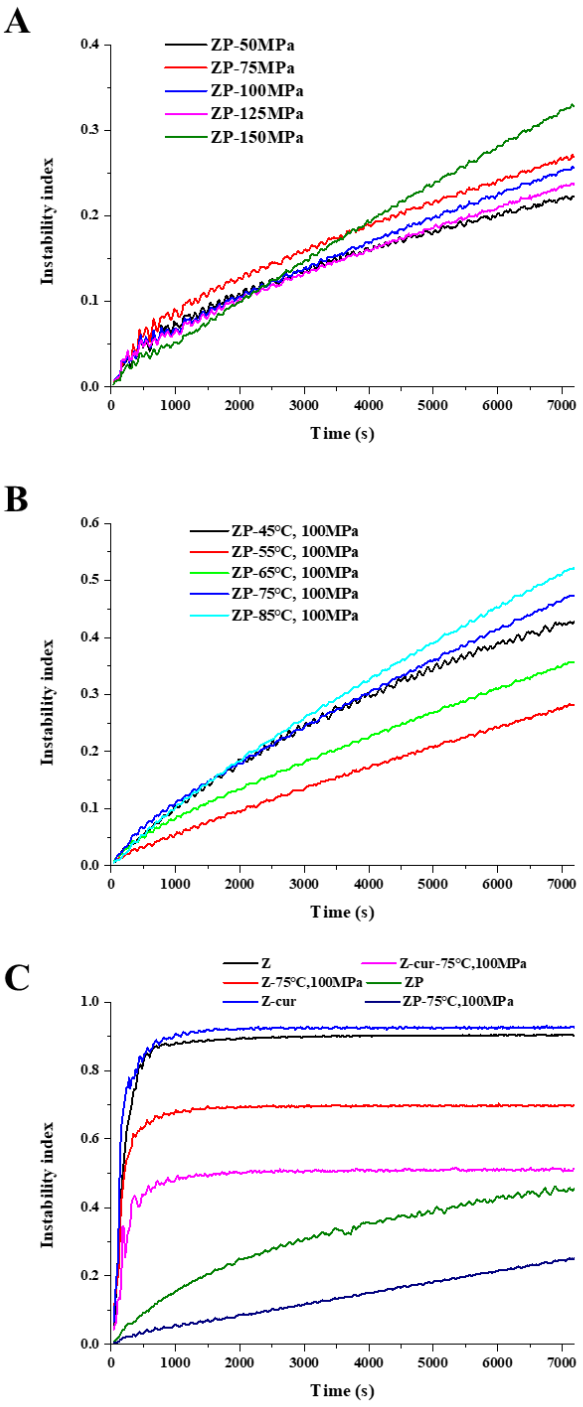
A
ZP-50MPa
ZP-75MPa
ZP-100MPa
ZP-125MPa
ZP-150MPa
Instability index
Time (s)
B
ZP-45°C, 100MPa
ZP-55°C, 100MPa
ZP-65°C, 100MPa
ZP-75°C, 100MPa
ZP-85°C, 100MPa
Instability index
Time (s)
C
Z
Z-cur-75°C,100MPa
Z-75°C,100MPa
ZP
Z-cur
ZP-75°C,100MPa
Instability index
Time (s)

Fig. 3

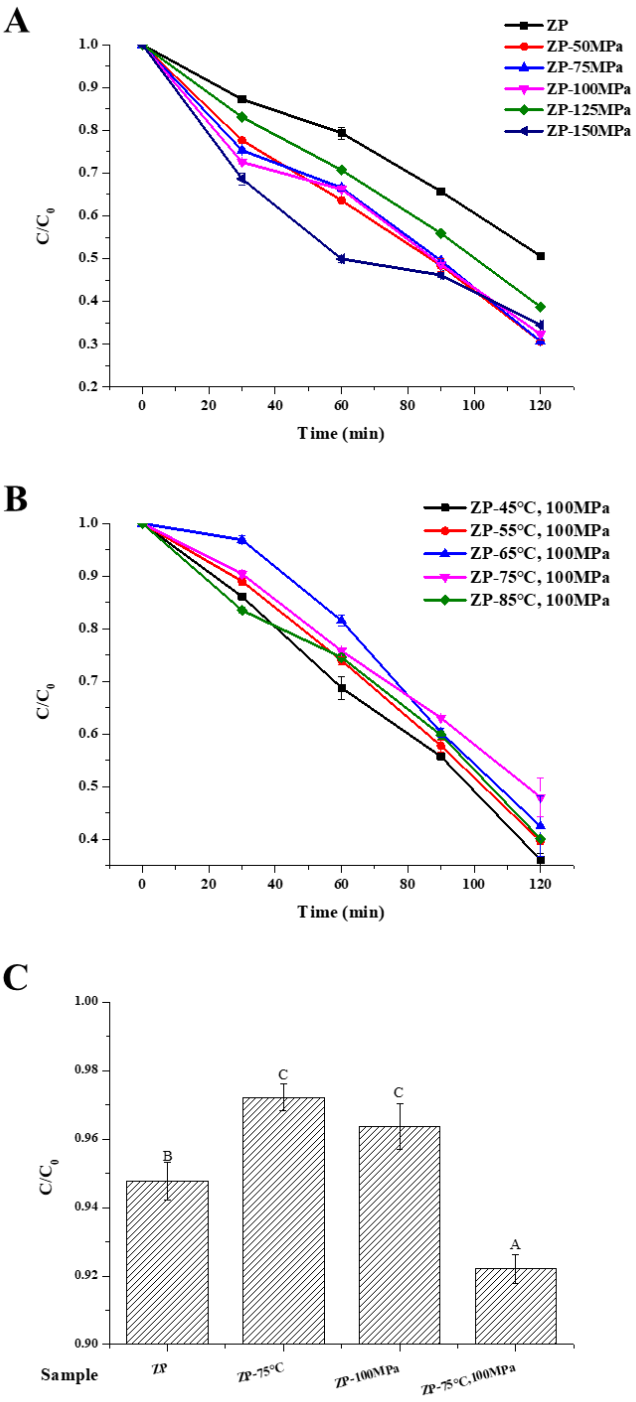
A
ZP
ZP-50MPa
ZP-75MPa
ZP-100MPa
ZP-125MPa
ZP-150MPa
C/C0
Time (min)
B
ZP-45°C, 100MPa
ZP-55°C, 100MPa
ZP-65°C, 100MPa
ZP-75°C, 100MPa
ZP-85°C, 100MPa
C/C0
Time (min)
C
C/C0
B
C
C
A
Sample
ZP
ZP-75°C
ZP-100MPa
ZP-75°C,100MPa

Fig. 4

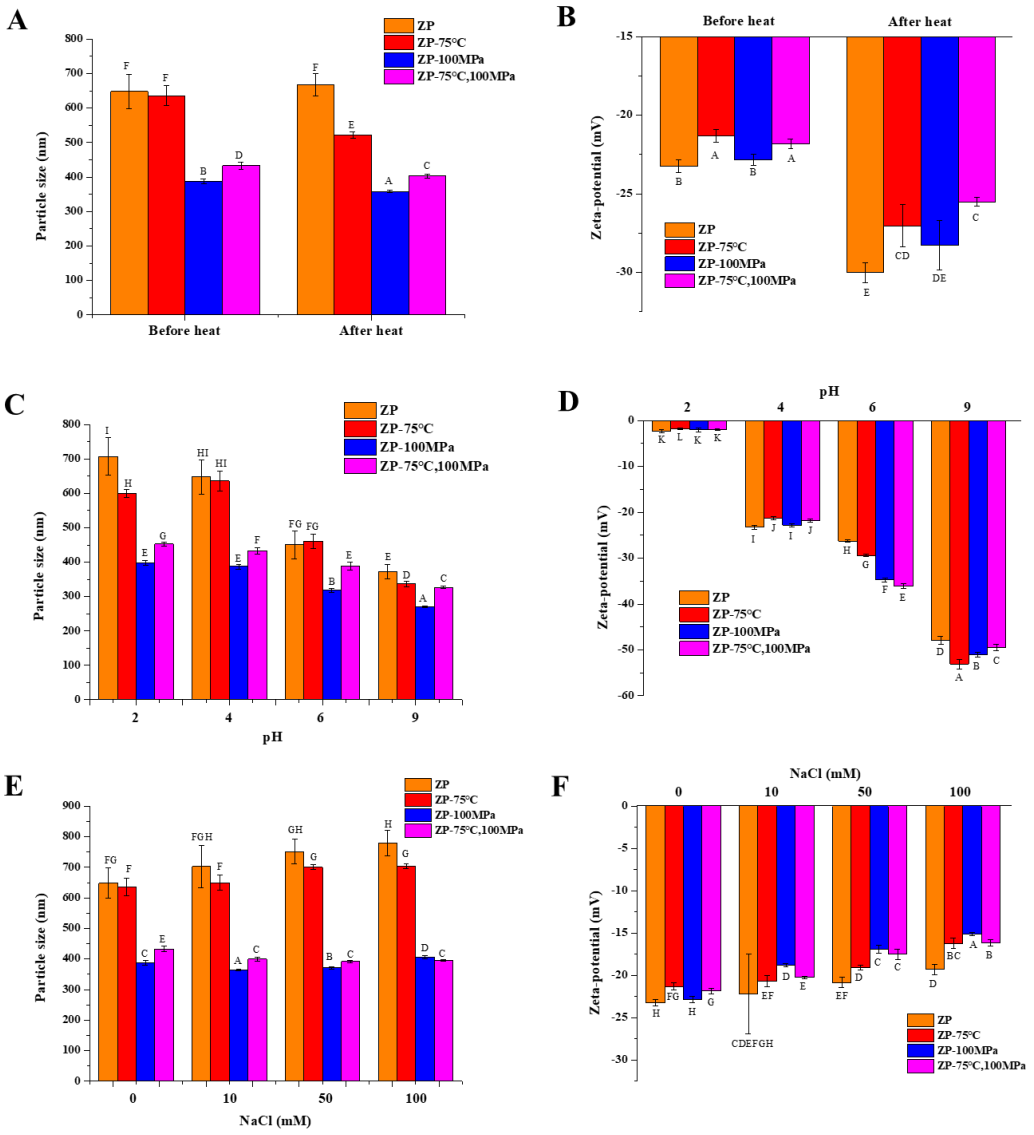
A
Particle size (nm)
ZP
ZP-75°C
ZP-100MPa
ZP-75°C,100MPa
Before heat
After heat
B
Zeta-potential (mV)
Before heat
After heat
C
Particle size (nm)
pH
D
Zeta-potential (mV)
pH
E
Particle size (nm)
NaCl (mM)
F
Zeta-potential (mV)
NaCl (mM)

Fig. 5

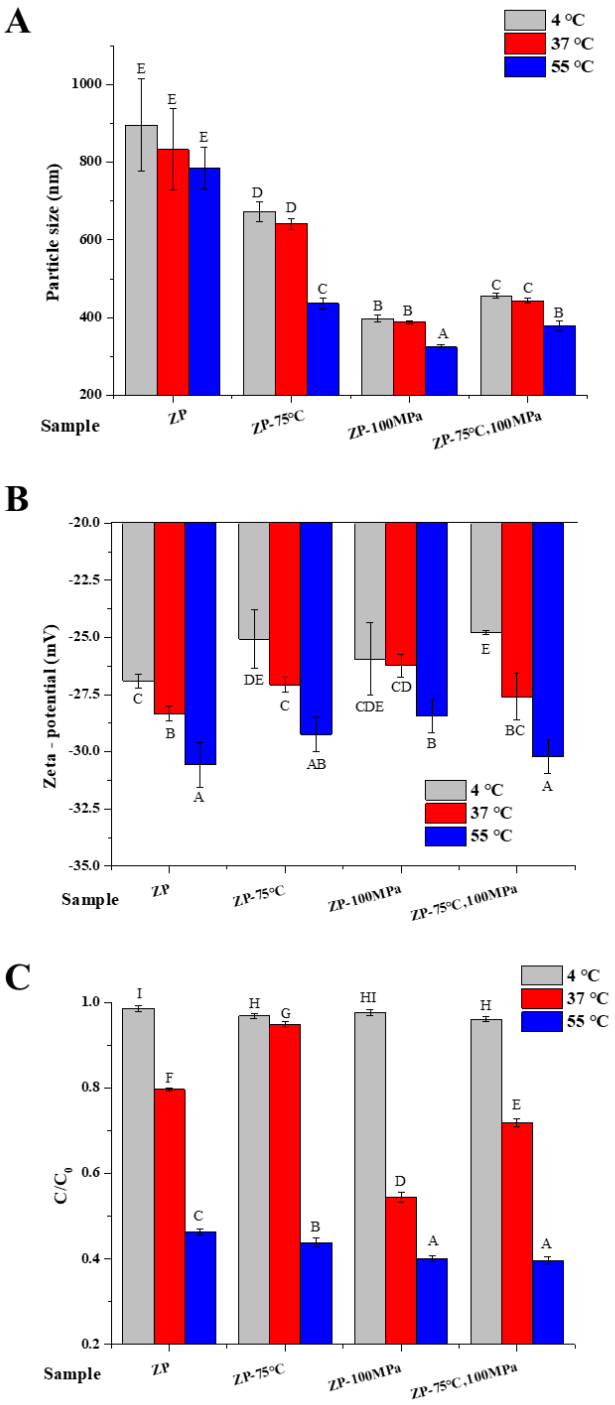
A
4 °C
37 °C
55 °C
Particle size (nm)
1000
800
600
400
200
E
E
E
D
D
C
B
B
A
C
C
B
Sample
ZP
ZP-75°C
ZP-100MPa
ZP-75°C,100MPa
B
Zeta - potential (mV)
-20.0
-22.5
-25.0
-27.5
-30.0
-32.5
-35.0
C
B
A
DE
C
AB
CDE
CD
B
E
BC
A
4 °C
37 °C
55 °C
Sample
ZP
ZP-75°C
ZP-100MPa
ZP-75°C,100MPa
C
4 °C
37 °C
55 °C
C/C0
1.0
0.8
0.6
0.4
0.2
I
F
C
H
G
B
HI
D
A
H
E
A
Sample
ZP
ZP-75°C
ZP-100MPa
ZP-75°C,100MPa

Fig. 6

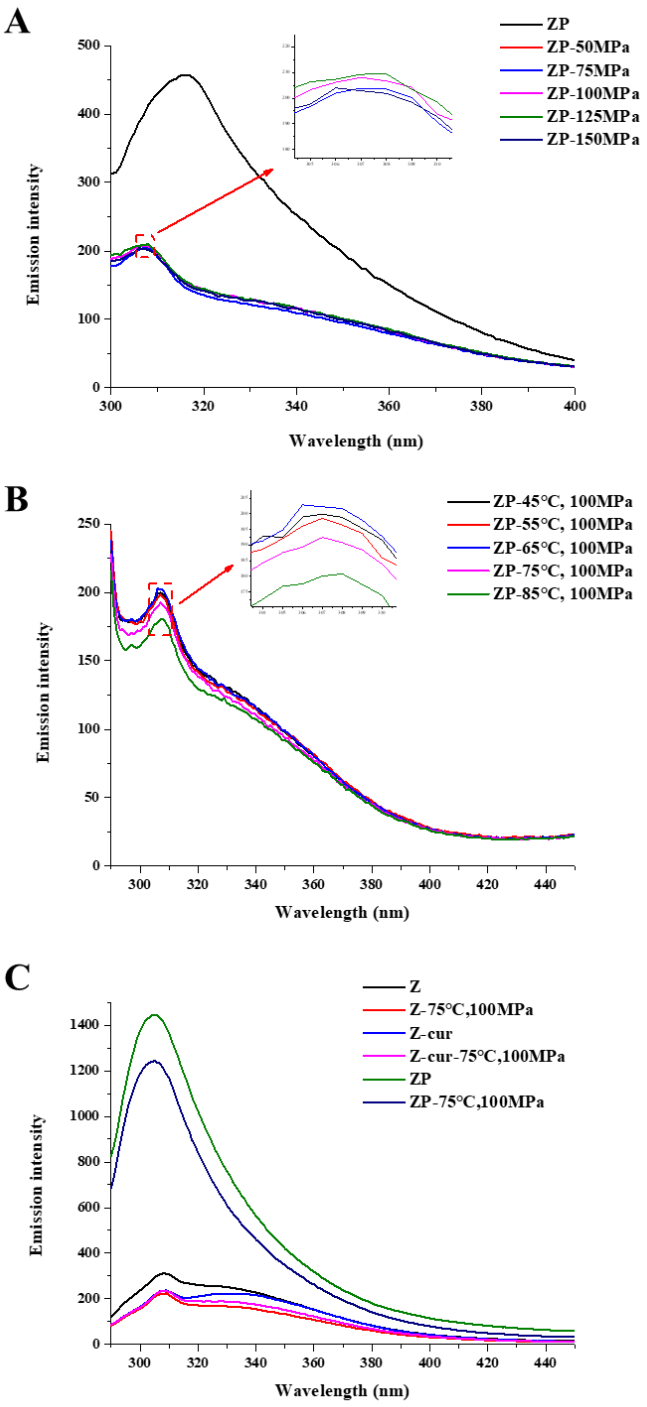
A
ZP
ZP-50MPa
ZP-75MPa
ZP-100MPa
ZP-125MPa
ZP-150MPa
Emission intensity
Wavelength (nm)
B
ZP-45°C, 100MPa
ZP-55°C, 100MPa
ZP-65°C, 100MPa
ZP-75°C, 100MPa
ZP-85°C, 100MPa
Emission intensity
Wavelength (nm)
C
Z
Z-75°C,100MPa
Z-cur
Z-cur-75°C,100MPa
ZP
ZP-75°C,100MPa
Emission intensity
Wavelength (nm)

Fig. 7

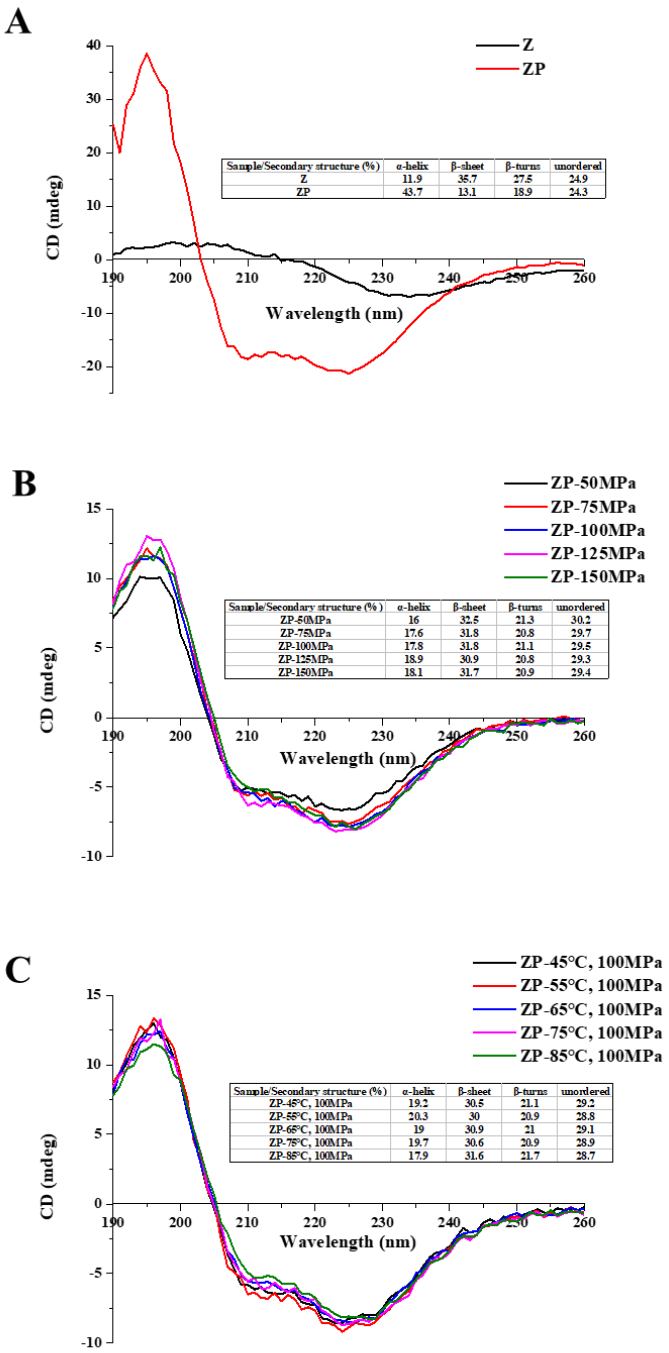
A
Z
ZP
CD (mdeg)
Wavelength (nm)
Sample/Secondary structure (%) | α-helix | β-sheet | β-turns | unordered
Z | 11.9 | 35.7 | 27.5 | 24.9
ZP | 43.7 | 13.1 | 18.9 | 24.3
B
ZP-50MPa
ZP-75MPa
ZP-100MPa
ZP-125MPa
ZP-150MPa
CD (mdeg)
Wavelength (nm)
Sample/Secondary structure (%) | α-helix | β-sheet | β-turns | unordered
ZP-50MPa | 16 | 32.5 | 21.3 | 30.2
ZP-75MPa | 17.6 | 31.8 | 20.8 | 29.7
ZP-100MPa | 17.8 | 31.8 | 21.1 | 29.5
ZP-125MPa | 18.9 | 30.9 | 20.8 | 29.3
ZP-150MPa | 18.1 | 31.7 | 20.9 | 29.4
C
ZP-45°C, 100MPa
ZP-55°C, 100MPa
ZP-65°C, 100MPa
ZP-75°C, 100MPa
ZP-85°C, 100MPa
CD (mdeg)
Wavelength (nm)
Sample/Secondary structure (%) | α-helix | β-sheet | β-turns | unordered
ZP-45°C, 100MPa | 19.2 | 30.5 | 21.1 | 29.2
ZP-55°C, 100MPa | 20.3 | 30 | 20.9 | 28.8
ZP-65°C, 100MPa | 19 | 30.9 | 21 | 29.1
ZP-75°C, 100MPa | 19.7 | 30.6 | 20.9 | 28.9
ZP-85°C, 100MPa | 17.9 | 31.6 | 21.7 | 28.7

Fig. 8

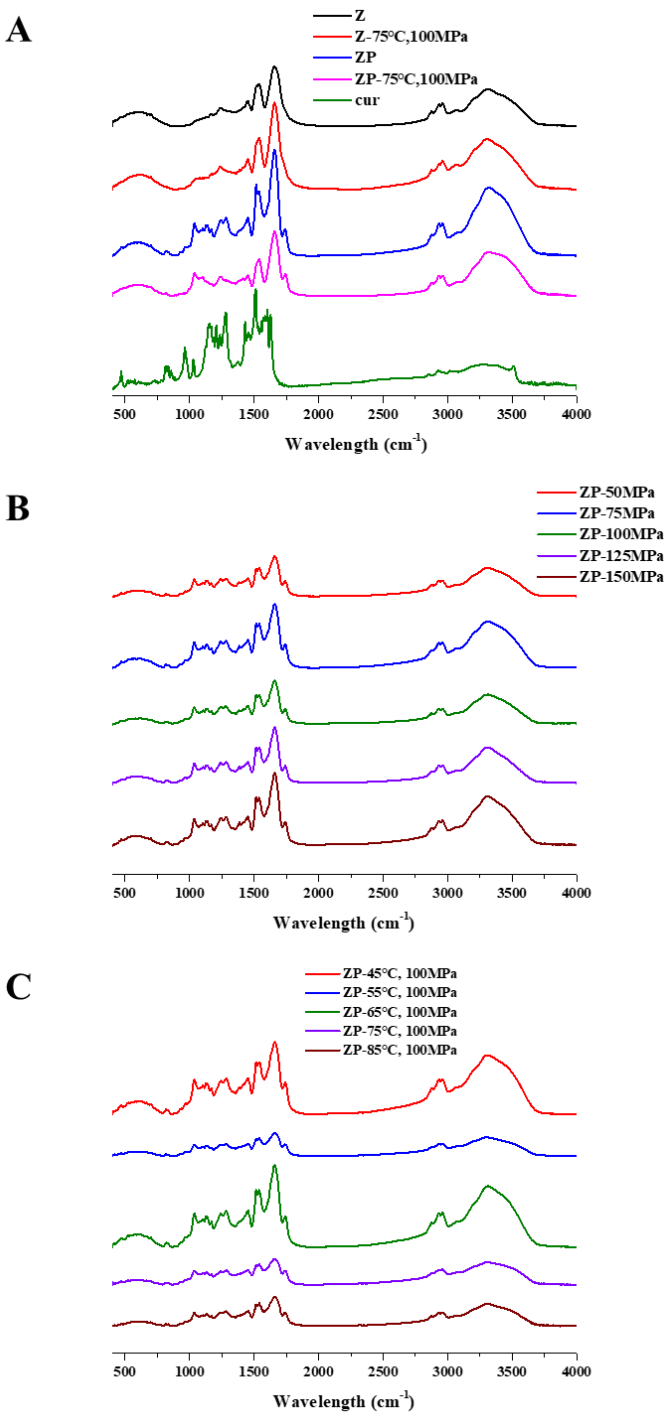
A
Z
Z-75°C,100MPa
ZP
ZP-75°C,100MPa
cur
500
1000
1500
2000
2500
3000
3500
4000
Wavelength (cm-1)
B
ZP-50MPa
ZP-75MPa
ZP-100MPa
ZP-125MPa
ZP-150MPa
500
1000
1500
2000
2500
3000
3500
4000
Wavelength (cm-1)
C
ZP-45°C, 100MPa
ZP-55°C, 100MPa
ZP-65°C, 100MPa
ZP-75°C, 100MPa
ZP-85°C, 100MPa
500
1000
1500
2000
2500
3000
3500
4000
Wavelength (cm-1)

Fig. 9

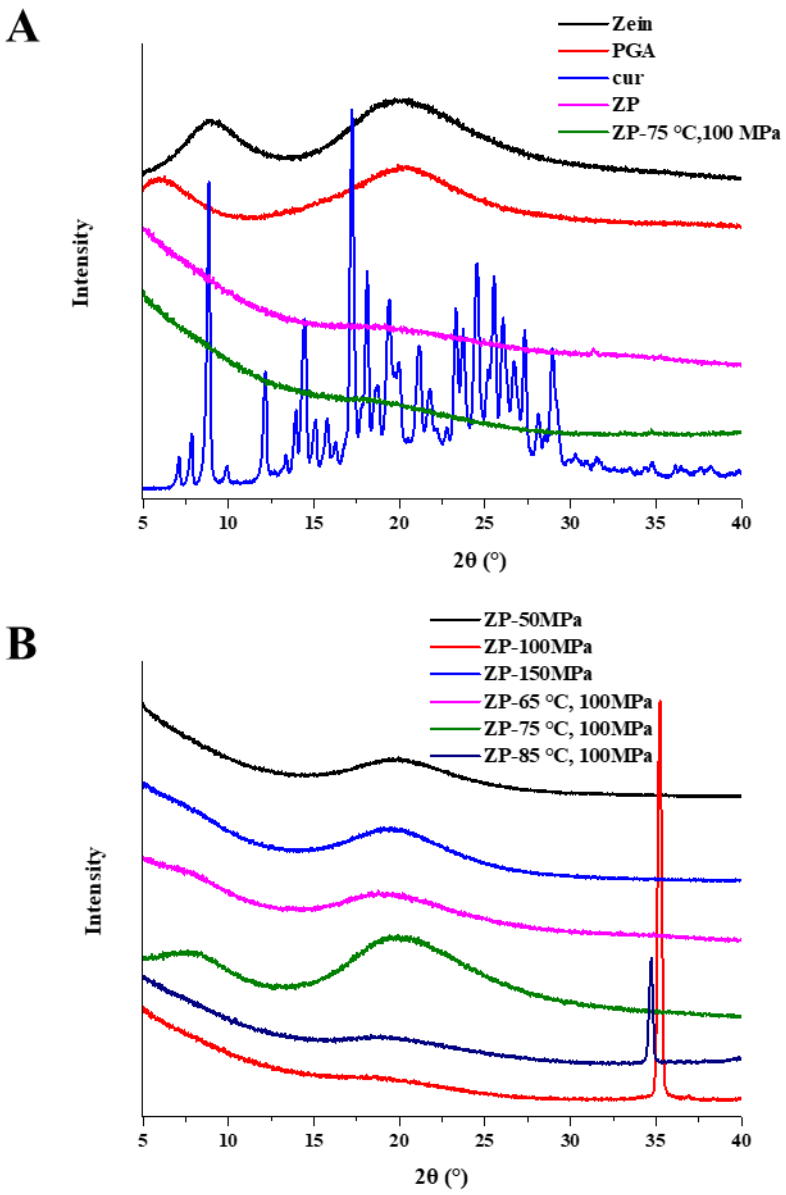
A
Zein
PGA
cur
ZP
ZP-75 °C,100 MPa
Intensity
5
10
15
20
25
30
35
40
2θ (°)
B
ZP-50MPa
ZP-100MPa
ZP-150MPa
ZP-65 °C, 100MPa
ZP-75 °C, 100MPa
ZP-85 °C, 100MPa
Intensity
5
10
15
20
25
30
35
40
2θ (°)

Fig. 10

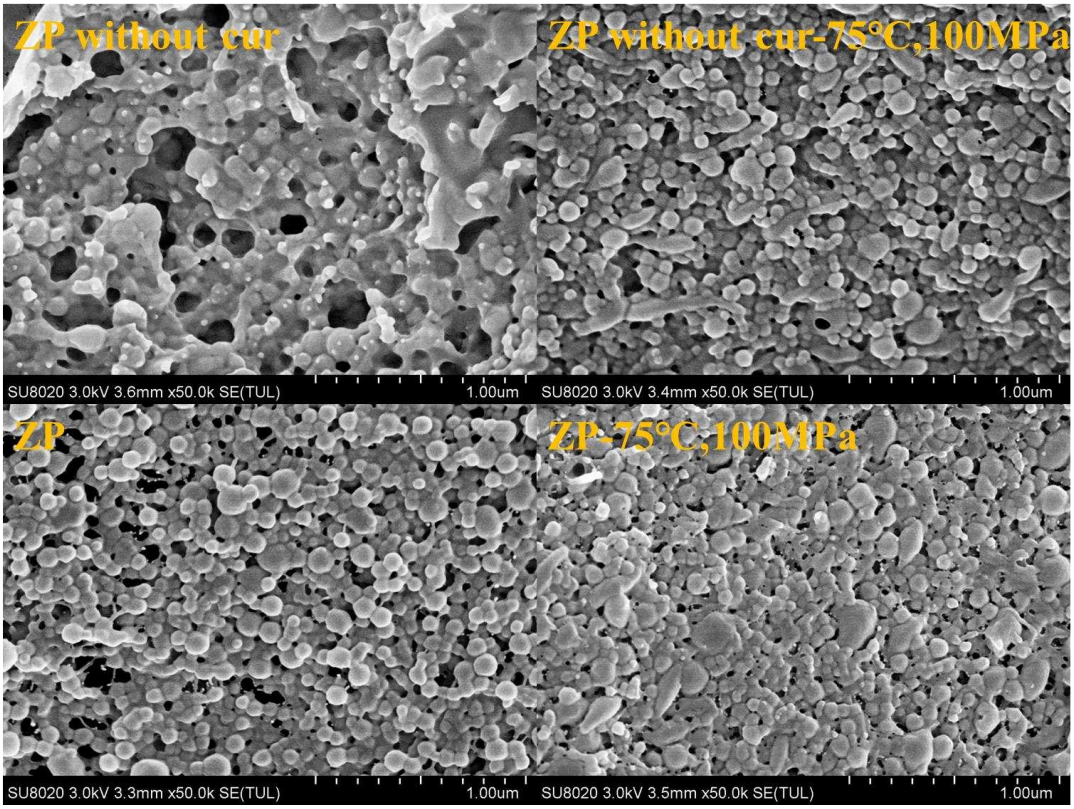
ZP without cur
SU8020 3.0kV 3.6mm x50.0k SE(TUL)
1.00um
ZP without cur-75°C,100MPa
SU8020 3.0kV 3.4mm x50.0k SE(TUL)
1.00um
ZP
SU8020 3.0kV 3.3mm x50.0k SE(TUL)
1.00um
ZP-75°C,100MPa
SU8020 3.0kV 3.5mm x50.0k SE(TUL)
1.00um

Fig. 11

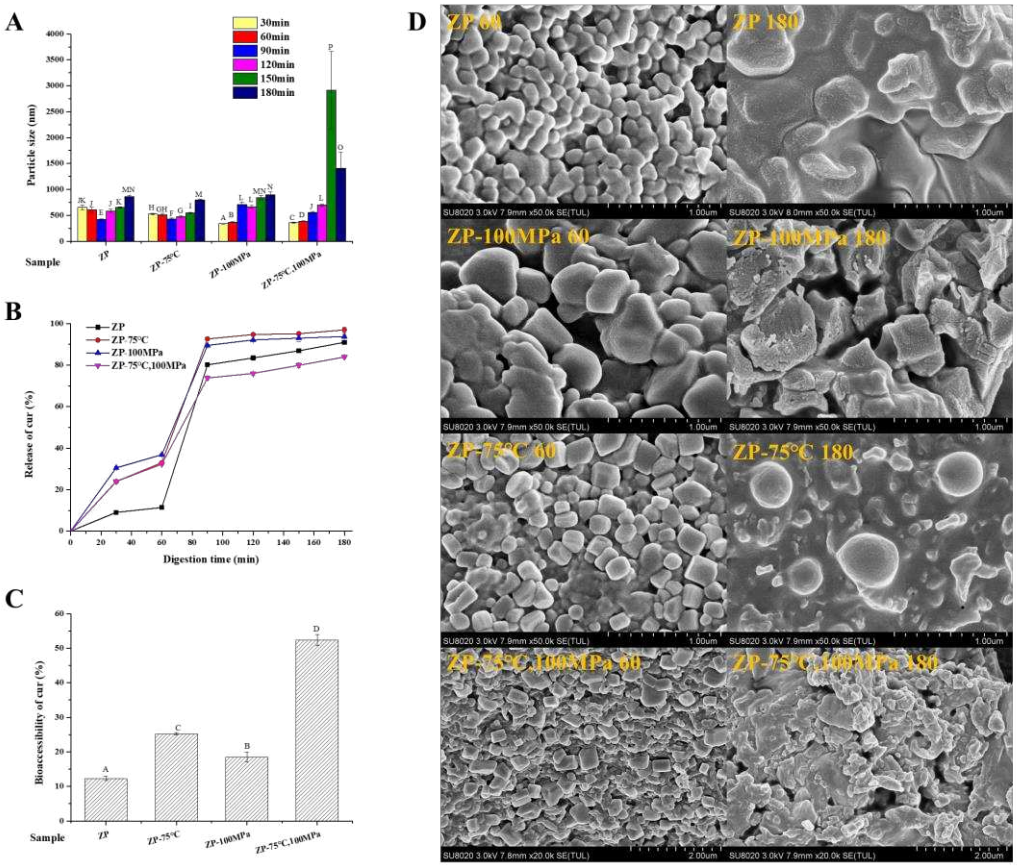
A
30min
60min
90min
120min
150min
180min
Particle size (nm)
Sample
ZP
ZP-75°C
ZP-100MPa
ZP-75°C,100MPa
B
ZP
ZP 75°C
ZP 100MPa
ZP 75°C,100MPa
Release of cur (%)
Digestion time (min)
C
Bioaccessibility of cur (%)
Sample
ZP
ZP-75°C
ZP-100MPa
ZP-75°C,100MPa
D
ZP 60
ZP 180
ZP-100MPa 60
ZP-100MPa 180
ZP-75°C 60
ZP-75°C 180
ZP-75°C,100MPa 60
ZP-75°C,100MPa 180

Fig. 12

Graphical abstract:

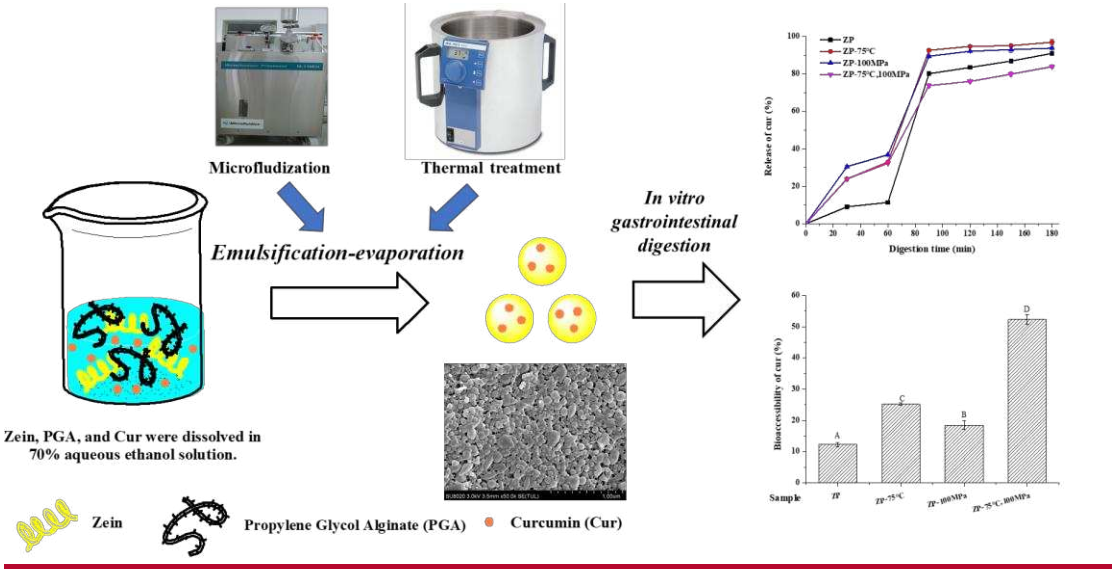

Author Contributions Statement:

Yang Wei: Conceptualization, Methodology, Software, Writing- Original draft preparation. **Chao Wang:** Data curation. **Xin Liu:** Software. **Alan Mackie**: Reviewing and Editing. **Liang Zhang:** Investigation. **Jinfang Liu:** Supervision. **Like Mao:** Software. **Fang Yuan:** Validation. **Yanxiang Gao:** Writing- Reviewing and Editing.

*Conflict of Interest form

Conflict of Interest

The authors declare no competing financial interest in this study.